Digital Manufacturing Techniques for Microfluidic Device Fabrication

Kurt Castro

A thesis submitted in partial fulfillment of the requirements for the degree of

Master of Science in Bioengineering

University of Washington

2018

Committee:

Albert Folch

Barry Lutz

Alshakim Nelson

Program Authorized to Offer Degree:

Bioengineering

University of Washington

Abstract

Digital Manufacturing Techniques for Microfluidic Device Fabrication

Kurt Castro

Supervisory Committee Chairperson: Dr. Albert Folch
Bioengineering

Microfluidic devices are currently used in a wide range of scientific and biomedical areas such as tissue engineering, cell biology, and implantable devices. Lab-on-a-chip research utilizing microfluidic devices has advanced significantly over the last decade and provides advantages of miniaturization, uniformity, accuracy, reproducibility, fluid/cell/tissue manipulations, rapid sample processing, and precise control of fluids.

Traditional methods of manufacturing microfluidic devices are based on semiconductor microfabrication technology. Specifically, a combination of photolithography and soft lithography have been used where devices are built by molding a transparent, elastomeric, and biocompatible material called polydimethylsiloxane. However, this fabrication process is extremely labor intensive, time consuming, expensive, not amenable for high-throughput manufacturing, and makes commercialization of microfluidic devices difficult. Digital manufacturing techniques centered around computers that automate the fabrication process are alternatives with high potential for reducing fabrication costs and time. Techniques such as laser micromachining and 3D printing, specifically stereolithography (SL), are explored in this research.

Laser micromachining was used to engrave microchannels onto plastic poly(methyl methacrylate) substrates and the channel dimensions were measured. Laser micromachining was then used to fabricate an all-plastic personalized drug testing microfluidic platform called OncoSlice that is meant to find the optimal subset of therapies specific for individual cancer patients. The device was composed of a 40-well plate that holds drugs and a channel network layer that delivers drugs to tissue samples. Optimization of laser settings to fabricate these layers was performed and several methods for bonding these layers together were explored.

A method that uses SL to print two materials together in a single print to create microchannels with integrated biosensors was also developed. Two resins were utilized: a microchannel resin and a biosensor resin. Both resins are based on poly(ethylene glycol) diacrylate polymerization chemistry. The biosensor resin was incorporated with biotinylated structures for biotin-binding assays. Three biosensor strips were printed within a microchannel and fluorescence microscopy was used to confirm the existence of biotin heads within the strips.

The digital manufacturing techniques used in this research to build microfluidic devices illustrate that fabrication time and costs can be significantly reduced. As laser micromachining and 3D printing systems becoming increasingly more advanced, microfluidic devices will become less expensive and simpler and convenient to produce.

Acknowledgements

Table of Contents

List of Figures

List of Tables

List of Nomenclature

Symbol	Section first used in	Description
PDMS	1.1	Polydimethylsiloxane
UV	1.2	Ultraviolet
CAD	1.2	Computer-aided design
CAM	2.1	Computer-aided manufacturing
SL	2.1	Stereolithography
CNC	2.2	Computer numerical control
ULS	2.3	Universal Laser Systems
DLP	2.4	Digital light processing
DMD	2.4	Digital micromirror device
STL	2.4	Stereolithographic
VLS	3.1	VersaLaser
PMMA	3.1	Poly(methyl methacrylate)
COC	3.1	Cyclic olefin copolymer
PET	3.1	Polyethylene terephthalate
PC	3.1	Polycarbonate
PCR	4.1	Polymerase chain reaction
PTFE	4.1	Polytetrafluoroethylene
PS	4.1	Polystyrene
R_H	4.3	Hydraulic resistance
η	4.3	Fluid viscosity

L	4.3	Length
R	4.3	Radius
w	4.3	Width
H	4.3	Height
Q	4.3	Volumetric flow rate
A	4.3	Cross-sectional area
v	4.3	Fluid velocity
IPA	4.4	Isopropyl alcohol
DI	4.4	Deionized
APTES	4.5	(3-aminopropyl)triethoxysilane
PSA	4.5	Pressure sensitive adhesive
PBS	4.5	Phosphate buffered saline
LSE	4.5	Low surface energy
PEG-DA	5.2	Poly(ethylene glycol) diacrylate
ITX	5.2	2-isopropylthioxanthone
TMSPMA	5.2	3-(trimethoxysilyl)propyl methacrylate
BSA	5.2	Bovine serum albumin
PEG	5.3	Poly(ethylene glycol)

1. Fabrication of Microfluidic Devices by Soft Lithography

1.1 Introduction

Microfluidics is a technology wherein liquids and gases are manipulated in channels having cross-sectional dimensions in the range of 10-500 μm. These miniaturized systems are commonly used for chemical, biological, and medical applications. The most common material used to fabricate microfluidic devices is polydimethylsiloxane (PDMS). The Whitesides group from Harvard was the first to utilize this material to fabricate microfluidic devices, and since then, over 200,000 studies utilizing this technique have been published[1]. Microfluidics has applications in a variety of fields such as molecular analysis, protein analysis, and cellular analysis. For example, it has been used to facilitate both DNA sequencing and point-of-care diagnostic assays, and it has been used to develop numerous cell culture platforms. Consequently, fabrication of microfluidic devices remains crucial.

1.2 Fabrication of Microfluidic Devices Using Photolithography and Soft Lithography

The conventional method of fabricating microfluidic devices uses a process called soft lithography which consists of replica molding PDMS using a master mold created using photolithography (Fig. 1)[2]. Microfluidic PDMS devices are divided into two categories: passive and active devices. Passive devices consist of a single molded layer of PDMS and function as flow splitters, reaction chambers, gradient generators, etc. Active devices consist of pumps and valves and are usually composed of several molded layers of PDMS. The Quake group from the California Institute of Technology was the first to develop PDMS microfluidic valves using multilayer soft lithography[3]. These valves consist of three layers of PDMS bonded together. The bottom layer is the flow layer where liquids and gases move within the device. The middle layer is a thin PDMS membrane. The top layer is the control layer that has channels that are placed perpendicular to the flow channels in areas where flow needs to be controlled. Pressurizing the control channels causes the thin PDMS membrane to deflect down and stop flow in the flow channels. Programming of the control channels allows for automated control of fluids.
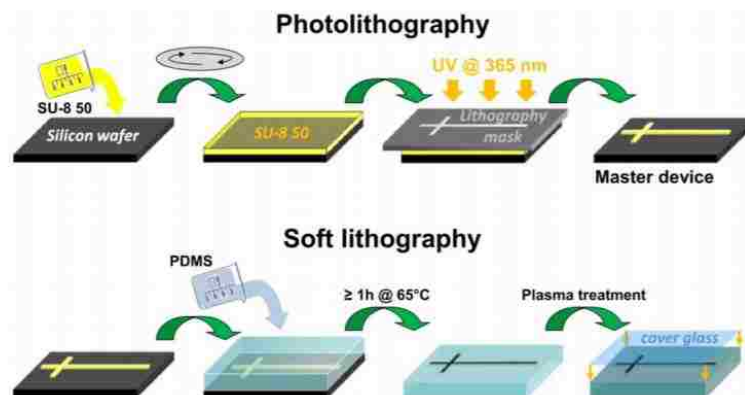
Figure 1: Fabrication of microfluidic devices using PDMS – image reproduced from Ref. 4 with permission from The Royal Society of Chemistry

The fabrication of PDMS-based microfluidic devices begins with the design of a lithography photomask. This mask acts as partial shield for ultraviolet (UV) light that is used in photolithography, an optical means of transferring patterns onto substrates. Masks are typically designed in computer-aided design (CAD) programs. A common type of mask is chrome on soda lime glass that is created using a laser writer. Masks are usually fabricated using a third-party manufacturer since most labs do not have the necessary tools to fabricate masks in-house.

Several methods for the fabrication of the master mold exist, but the most common one utilizes an epoxy-based, negative photoresist called SU-8 spin-coated onto a silicon wafer. The wafer is exposed to UV light through the photomask such that the pattern on the mask is transferred to the resist. Areas of SU-8 exposed to the UV light polymerize and solidify. Unexposed, and therefore unpolymerized, areas are removed using a developer leaving positive features behind on the wafer.

PDMS pre-polymer is then prepared by mixing the PDMS base with a curing agent at a ratio of 10 to 1, respectively. The pre-polymer is poured over the master mold and cured at 65˚C for 2 hours. The cured PDMS is then carefully peeled from the wafer and the positive features of the mold are embossed as negative features on the PDMS and form channels. The PDMS molded channels at this point are open and are either bonded to a glass slide or another layer of PDMS to close them. This is done by treating the PDMS and/or glass slide with oxygen plasma at 660 mTorr for 1 minute and then bonding the layers immediately by manual pressure. For multilayered devices such as those that contain pneumatically controlled valves or those that have channels that follow 3D architecture, precise alignment is required to ensure a proper working device, so alignment and bonding steps are crucial.

1.3 Limitations of Soft Lithography

PDMS-based microfluidic devices are the most commonly used type of devices because PDMS is elastomeric, optically clear, biocompatible, and inexpensive. However, the fabrication procedure for these devices, which involves a combination of soft lithography and photolithography, is cumbersome[5]. Fabrication is labor intensive and requires highly-skilled personnel with significant expertise, specialized fabrication facilities such as cleanrooms, and bulky, expensive instruments. Simple devices can take 24 hours to fabricate with multiple design iterations increasing costs due to the need to create new molds. Multilayered devices are even more complex and can take several days to fabricate since each layer requires its own mold and photomask. Furthermore, they are prone to failure due to the need for precision alignment.

Other high-throughput methods of manufacturing microfluidic devices are needed and are explored here. These methods are based on digital manufacturing and rapid prototyping where the user designs a device using CAD software and their design is sent to a manufacturing tool that entirely or partially automates the fabrication process. These methods are less labor intensive, faster, require little to no assembly, and require less expertise.

2. Digital Manufacturing Techniques

2.1 Introduction

Digital manufacturing is an integrated approach to manufacturing that is centered around computers. Following the development of CAD programs, computer-aided manufacturing (CAM) systems were created[6]. CAD software is used to design parts and assemblies which are then sent as files to CAM systems such as milling machines, laser cutters, or 3D printers (Fig. 2). These manufacturing tools interpret the design files and automate the fabrication of the designed parts and assemblies. Compared to conventional photolithography and soft lithography methods, digital manufacturing offers several advantages such as faster production time, decreasing costs, and less complicated assembly.

CAD Design   **Manufacturing Tools**   **Finished Part**

Figure 2: Digital microfluidic manufacturing process flow

Use of these manufacturing tools for microfluidic device fabrication requires less hands-on time since the bulk of the manufacturing is automated. The many steps involved in conventional microfluidic device fabrication such as the generation of masks and molds, spinning photoresist, and the many baking steps are eliminated in a digital manufacturing process.

Multilayered PDMS microfluidic devices such as devices that have integrated control valves require a contact aligner to ensure that the valves are placed in the intended positions. Otherwise, the device would not function as designed and the fabrication would have to start from the beginning. For this reason, experienced and highly-skilled personnel are needed to fabricate complex multilayered microfluidic devices. Digital manufacturing, however, eliminates this need since alignment can be fully or partially automated depending on the manufacturing tool and expertise is more easily transferable between personnel. A high level of flexibility is provided by digital manufacturing because the manufacturing tools use digital data that can be easily and rapidly changed allowing for design iterations to be produced faster.

There are three types of digital manufacturing techniques that will be discussed in this research: micromilling, laser micromachining, and a type of 3D printing called stereolithography (SL). The applications of each in fabricating microfluidic devices will be described as well as the advantages and disadvantages of each.

2.2 Micromilling

Micromilling is a subtractive manufacturing process that removes material from substrates using rotating cutting tools. A basic micromill consists of a worktable to position substrates, a rotating cutting tool called an endmill, and an overhead spindle that secures the endmill (Fig. 3). Endmills are similar to drill bits, but endmills are primarily used to cut parallel to a planar surface of a substrates while drill bits cut axially and perpendicular to a substrate. Modern mills are automated using computer numerical control (CNC) which determines the sequence of machine control commands that the mill follows to produce a desired design. CNC mills convert CAD models to finished parts by automating movement of the endmill, spindle speeds, and cutting depths. This type of automation allows for increased repeatability and reduced human error.
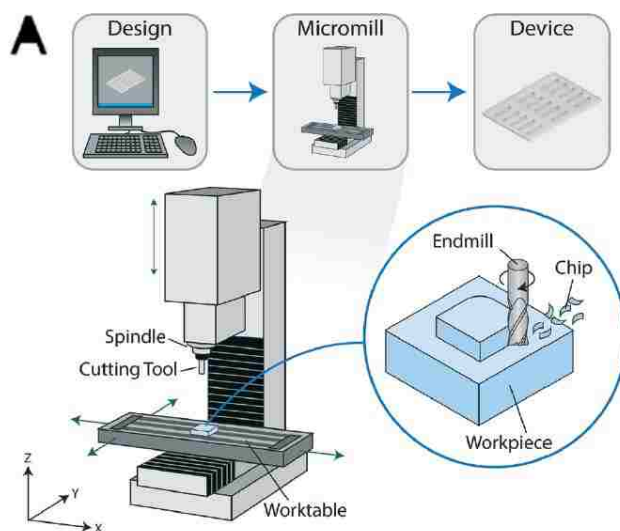
Figure 3: Components of a CNC micromill and the process to produce microfluidic devices - image reproduced from Ref. 7 with permission from The Royal Society of Chemistry

Micromilling offers several advantages. Firstly, it precludes the need to create a lithographic mask and a master mold and is therefore a maskless process. This advantage allows for shorter time between iterative designs since design changes that are made in a CAD file are directly translated to fabrication. Secondly, endmills with different profiles are available, so channels with different profiles can be produced in a single device. Milling settings can also be adjusted so that the endmills can cut channels of different depths, which is difficult to achieve with soft lithography. Another advantage of micromilling is that it can process a variety of materials, especially different plastics, so users can choose materials most appropriate for their applications. There are several manufacturers of CNC mills each with differing costs, work envelopes, speeds, and accuracies. For accuracies between 1 and 10 μm, most mills cost between $60,000 and $80,000[7]. There is also the Tormach PCNC 770 mill, however, that costs $15,500 and has an accuracy of 15 μm [7]. This is comparable to other digital manufacturing tools such as laser cutters, however, depending on the feature sizes desired by the user, the cost of a micromill varies.

Micromilling is certainly an attractive alternative to soft lithography, but it does have many drawbacks. Endmills with fine points are available and allow for features several microns in size

4

to be manufactured, and automation of micromills allow devices to be fabricated in less than an hour for simple designs. Performance Micro Tool, a vendor of precision drill bits and endmills, offers endmills that are only 5 μm in diameter allowing for microscale features of this size to be machined onto plastic. However, a single endmill with this diameter costs $180 and would need a high frequency of replacement since such a fine point is prone to damage and wear with each use rendering different channel feature dimensions after a long period of use. The cost of maintaining such a microfluidic fabrication system increases with each need to replace endmills. Additionally, micromilling is a slow process compared to other techniques and it creates highly rough surfaces that limit optical clarity which is critical for certain applications such as phase contrast cell microscopy. Layering and bonding of milled substrates to create channels that have 3D architecture is also still necessary. Thus, for micromilling to become a reliable method for high-throughput microfluidic device manufacturing the cost of precision endmills must be reduced or the durability of such endmills must be increased, and the high surface roughness that results must be reduced.

Overall, micromills are useful tools for creating microchannels directly in devices and provide an advantage of fast prototyping. However, it has certain limitations that make it less attractive than other tools. The costly maintenance of precision endmills, the slow processing speed, and high surface roughness hinder its applicability for high-volume production of microfluidic devices.

2.3 Laser Micromachining

Similar to micromilling, laser micromachining is also a subtractive process that uses a focused laser beam to ablate and vaporize material in a substrate. A laser micromachining system is composed of a cutting table, a laser optics system, a gas laser source, a fume extraction and air filtration system, and a gas assist to cool substrates and blow away debris as the laser engraves or cuts (Fig.4). Computer software converts designs from a CAD file into movements of the laser across the substrate to cut or engrave using CNC. The focusing depth of the laser, its power, and speed with which it moves can all be easily defined by the user to create different sized features. This type of automation also allows for increased repeatability and reduced human error.
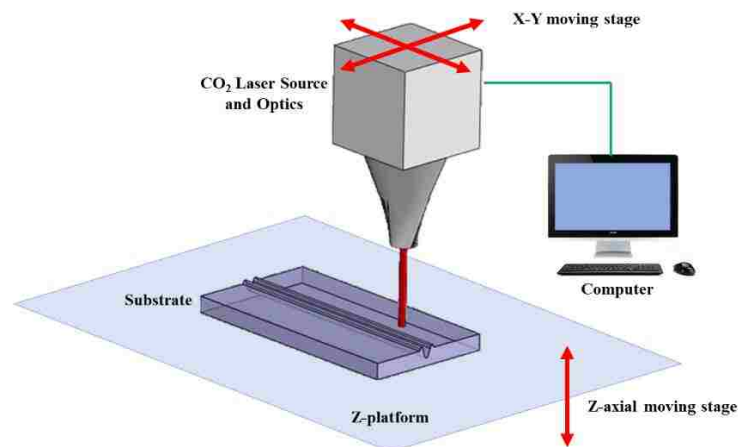
Figure 4: Schematic of a CO_2 laser system for building microfluidic devices - image adapted from Ref. 8 with permission from Springer Nature

Substrates are secured onto a cutting table, and using computer software, the laser can be focused to different depths in accordance with the thickness of the substrate. The laser cutter converts line patterns defined in a CAD file into movements of the laser across the substrate. Each line(s) can be specified to have a specific laser power setting and a specific speed setting thereby producing features of different dimensions on a single substrate, which is difficult to do with soft lithography. The power setting is usually defined as a percentage of the maximum laser power of the system. The speed setting is also defined as a percentage of the maximum speed of the system. In general, more power and slower speeds lead to deeper and wider dimensions and vice versa.

Laser cutters and micromills have similar advantages. Both are maskless and both can process a variety of materials. Laser cutters have large work envelopes, so it is possible to create many copies of a device in one run of the machine. Compared to micromills, laser cutters have faster processing speeds and are also less expensive. A Universal Laser Systems (ULS) desktop 30 W laser system with all essential accessories costs about $12,000, which was determined by obtaining a quote from a local distributor. A laser system also requires less maintenance compared to micromills since the laser optics and filters in the filtration system do not have to be replaced as frequently as endmills. Laser optics are cleaned usually between every 3 months to a year depending on the frequency of use, and filters are usually changed every one to two years.

As with micromills, laser cutters also have disadvantages. Limited channel profiles are available with laser cutters since most laser beams have a Gaussian shape. Consequently, laser micromachined channels have this same shape. They are not able to produce other profiles such as square and rectangular channels. Reproducibility of channel profiles can also be an issue depending on the precision of the beam positioning system and the laser focusing system. Surface roughness is also an issue with laser micromachined channels, though exposing the channels to solvent vapors has been shown to alleviate this problem and increase optical quality[20]. Furthermore, creating channels with 3D architecture is also difficult due to the need for layering and bonding. The reliability of these bonding methods is critical since it directly affects device performance. Adding active components such as valves and pumps to laser micromachined microfluidic devices also remains difficult. The bonding of stiff, polymeric substrates to elastomeric materials such as PDMS to create Quake valves, for example, adds more assembly steps and may require surface modification techniques to be able to bond the two dissimilar materials.

Overall, laser micromachining provides a more efficient method of creating microfluidic devices than micromilling. Lasers can create features of different widths and depths on a single layer of a substrate without the need to remove and attach parts. Maintenance of a laser system is also less costly than a micromill. However, different components of a microfluidic device may still need to be assembled which may require skilled, experienced personnel to perform though less skill is needed than with soft lithography. Other digital manufacturing techniques such as 3D printing may preclude the need for assembly entirely.

2.4 Stereolithography

SL is an additive 3D printing process wherein parts are printed layer by layer using a process called photopolymerization. SL systems consist of a laser or digital light processing (DLP) system that selectively exposes photopolymer resin contained in a vat with UV light (Fig. 5)[5]. Parts are usually printed in the upside-down bat configuration. A build stage or plate moves down a pre-defined distance away from the transparent bottom of the vat. UV light directed by a digital micromirror device (DMD) causes chains of molecules to link (polymerize) and form a solid polymer in designed patterns between the bottom of the vat and the build plate. The build plate then moves up and then down to print the next layer. This repeats until the part is fully printed.

SL printers fabricate parts based on 3D CAD files created with 3D modeling software. Files are exported to the printer as a stereolithographic (STL) file. The printer then slices the part into layers. The number of layers is determined by the overall part thickness and the layer thickness that is set by the user. Each layer is polymerized either with a UV laser that "writes" across the resin or through images that are projected with a DLP system onto the resin. Depending on the part thickness, the printing time can vary.
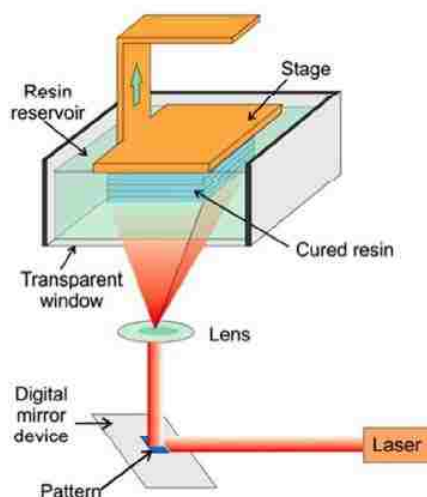
Figure 5: Schematic of a stereolithographic 3D printing system - reprinted with permission from *Anal. Chem.* 86, 7, 3240-3253. © Copyright 2014 American Chemical Society.

To create microchannels, the walls and roofs of the channels are polymerized by UV light and the uncured resin trapped within the channels is then flushed out. This process is highly automated and precludes the need for burdensome, complex device assembly. It has the advantage of being able to create channels with 3D architecture without the need for user alignment and bonding. Additionally, SL has previously been used to fabricate fluidic valves and pumps, inlet and outlet connectors directly printed onto a device for connection with off-device components[9-10], and modular microfluidic circuits[11-13]. Fully functional microfluidic devices can be created at a push of a button. This gives SL a huge advantage over micromills and laser micromachining systems. SL systems are also inexpensive. Systems such as the Asiga PICO 2, Formlabs Form 2, and Full Spectrum Laser's Phoenix Touch Pro are all under $15,000[14-16].

However, certain limitations do exist for SL systems. The minimum feature that can be printed is limited by the pixel size of the DLP system. Most SL systems have a 50 μm X/Y pixel resolution meaning that 50 μm is the minimum width a printed microchannel can have. As smaller pixel sizes become available in the near future, smaller microchannels can be fabricated. The size of the build plate also limits the size of printed devices. Larger devices would have to be fabricated by other means. Additionally, biocompatible, optically clear, and chemically resistant polymer resins are still being developed and characterized, so there is a limited material set available for SL-printed microfluidics. Optimal UV light exposure times also must be calibrated to obtain open channels for the user-defined layer thickness. Otherwise, clogged channels may form due to overexposure of roof layers or channels may not form at all due to underexposure. Photopolymerizable resins for microfluidics is currently a burgeoning research area that is continuing to make advancements.

Overall, SL may not be able to produce as small a feature as other digital manufacturing systems, but with continued advancements with optical components in printers and resin photochemistry it is possible that SL can become comparable or even more sophisticated than these systems. SL's main advantage over micromills and laser cutting is that it is an assembly-free platform. An entire microfluidic device can be designed in one CAD file and fabricated within one print. With other digital manufacturing methods, the user may need to fabricate components separately and assemble them together manually. This increases fabrication time and costs which is the reason for 3D printed microfluidics becoming a popular research topic. Ultimately, it has been observed through the research presented here that laser micromachining and stereolithography are more applicable for high-throughput microfluidic device fabrication than micromilling.

3. Laser Micromachining Characterization

3.1 Introduction

In previous studies, the size of microchannels micromachined with a laser usually had widths greater than 200 μm and depths greater than 50 μm. The challenges that this research has tried to address is being able to fabricate microchannels with smaller dimensions with a commercial laser cutting system.

The laser cutter used in this thesis was the VersaLaser (VLS) 3.60 system by ULS (Fig. 6). It has a work envelope of 610 x 305 mm, a maximum laser power of 30 W, a fume extraction system, and a lateral gas assist that directs air along the material's surface at an angle to remove laser processing byproducts. The system uses a 10.6 μm wavelength CO_2 infrared laser source.

The most common substrates used to build microfluidic devices by laser micromachining are plastic polymers since they are inexpensive compared to more commonly used substrates for microfluidic devices such as glass and silicon. Common polymers that have been used to micromachine microfluidic devices are poly(methyl methacrylate) (PMMA), cyclic olefin copolymer (COC), polyethylene terephthalate (PET), and polycarbonate (PC)[17]. PMMA was chosen for this research because it is biocompatible, has excellent optical transparency, low gas permeability, and is less expensive than PDMS. It has a high absorbance in the infrared range with a low heat capacity and low heat conductance allowing it to melt quickly. Upon application of heat, PMMA decomposes and vaporizes into volatile products such as its monomer methyl methacrylate leaving behind clean structures, while other polymers will burn and leave soot that is hard to remove[18-19].

Other lasers that can create microstructures within polymers are UV excimer lasers. They can produce features much smaller than features created with a CO_2 laser, but they are significantly more expensive. UV lasers also have low pulse frequencies and slow machining speeds making CO_2 lasers more appropriate for rapid manufacturing[22].

Figure 6: VLS 3.60 laser system. (A) Laser system and peripheral components. (B) Laser source and optics along with lateral gas assist and mechanism of movement across substrate.

3.2 Design and Fabrication Procedure

Designs must first be created using two-dimensional CAD drawing software such as AutoCAD by Autodesk. Features are usually color-coded to signify features to be cut with a specific power and speed setting and whether they are to be vector cut or raster engraved. Vector cutting involves laser cutting the outline of a shape or lines on a piece of material. Raster engraving involves the laser cutting material in a scanning fashion like an inkjet printer (Fig. 7). Two-dimensional designs are usually input into special software programs that control the laser. With this software, the user can determine where to place the design on the cutting bed, change power and speed settings according to the color of features in the sketch, and decide the order in which features are cut.

10

Vector cutting utilizes vector images which uses geometric formulas to describe the shape or outlines of features in the image. The laser traces the vector lines in the image to cut out the user's design. Vector cutting produces lines with small cross-sectional area dimensions. The width and depth of vector cuts depend on the user-defined laser speed and power settings. Higher power and lower speeds give larger widths and depths and vice versa. In order to make vector engravings, the lineweight for lines to be vector engraved must be set to 0 mm. Otherwise, the laser cutter will not cut these lines at all.

Raster engraving involves the laser moving back and forth across the material while it engraves an image. It engraves closely spaced vector lines to create wider features. It mainly utilizes raster images which are composed of pixels, so it is resolution dependent. The dots per inch or pixels per inch in the raster image directly affects the level of detail that will be imprinted onto the material. Raster engraving can produce higher aspect ratio channels with the same depth but varying widths. Varying widths of lines in is done by changing the lineweight of lines to anything greater than 0 mm in a CAD drawing.
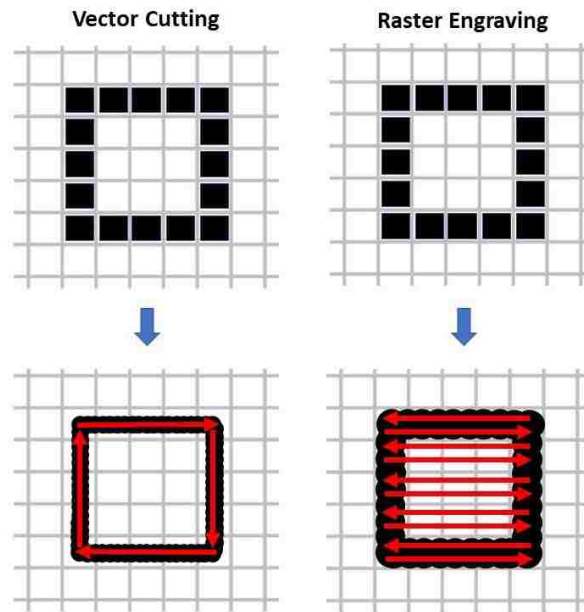
Figure 7: Difference in laser movement across substrates for vector cutting and raster engraving

Before placing material into the cutting bed of the laser, the thickness of the material must be determined and input into the laser control software. With this information, the laser system will automatically focus to the top of the material. Without this information, the laser will product inaccurate cuts or the optics system may be damaged if it collides with the material to be processed.

3.3 Vector Cut Characterization

As previously mentioned in Section 3.2, the dimensions of features fabricated onto a material's surface is determined by the power and speed setting of the laser. To determine if small channel dimensions can be fabricated with the VLS 3.60, vector cuts created with different combinations of power and speed settings were engraved onto a 3.1 mm thick sheet of PMMA. Power and speed

11

settings are set as percentages of the laser cutter's maximum values. The VLS 3.60 maximum power is 30 W. Its maximum vector speed is 254 mm/s and its top raster speed is 1270 mm/s. All possible combinations of speed settings of 20%, 40%, 60%, 80%, and 100% and power settings of 2%, 4%, 6%, 8%, 10%, and 12% were used to engrave designed line patterns (Fig. 8A). Only certain combinations of speed and power settings were able to produce contiguous channels and the dimensions of these channels were measured under a light microscope. The channel widths and depths are displayed in Fig. 8C and 8D. A general trend of higher powers and slower speeds yielding channels with higher cross-sectional areas can be observed which is intuitive. The channel widths ranged from 50 to 120 μm and the channel depths ranged from 25-160 μm, which are smaller dimensions than previously achieved in previous studies. High aspect ratio features cannot be readily achieved with vector cuts (Fig. 8E). However, raster cuts can provide higher width to height aspect ratios.

A

B

C

D

12
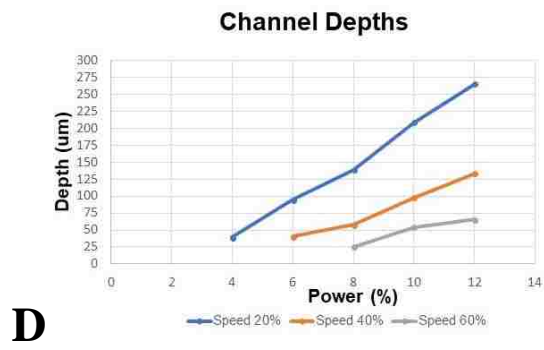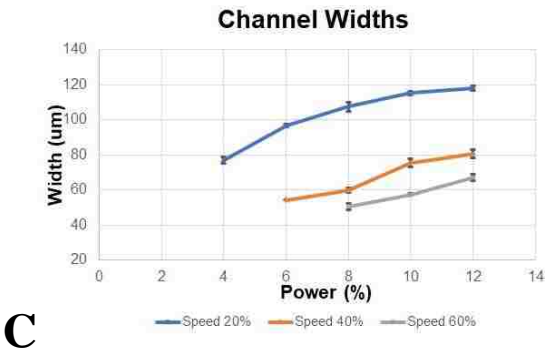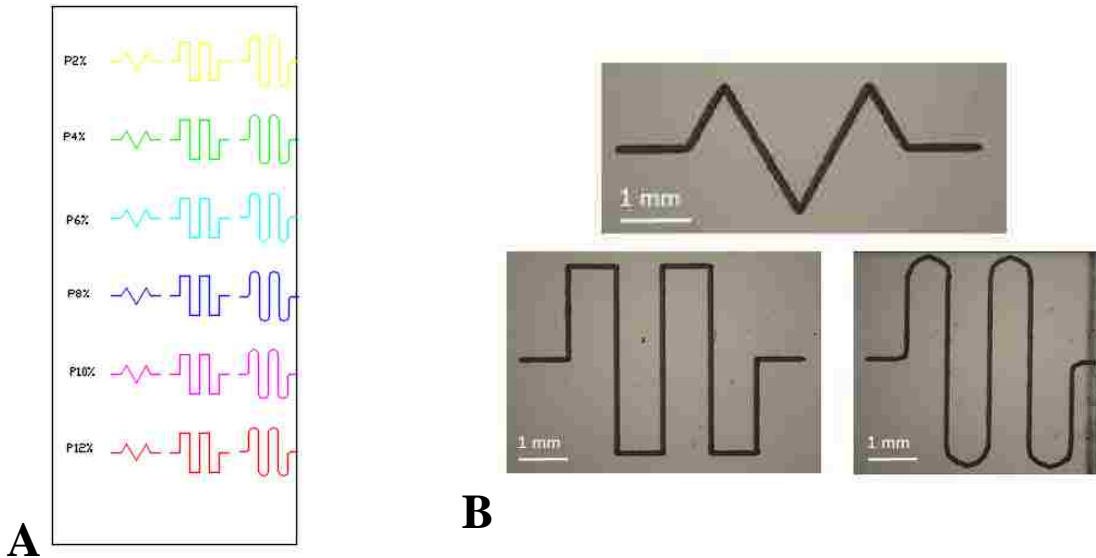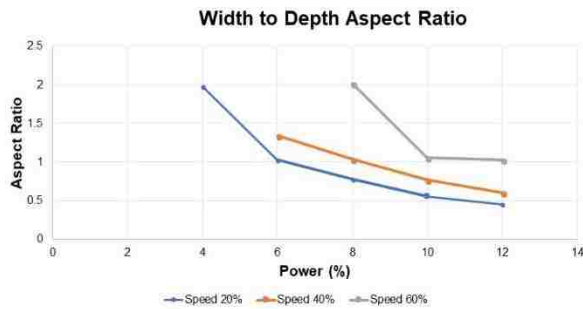
E
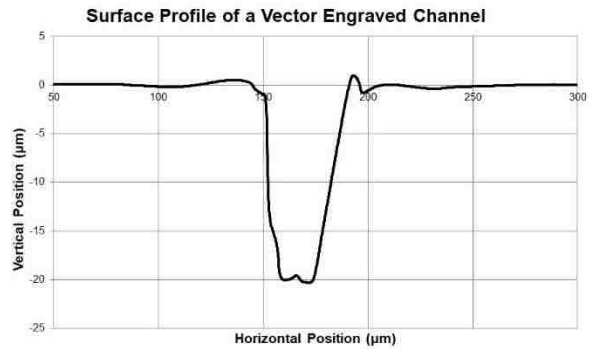
F

Figure 8: Vector cutting characterization with VLS 3.60. (A) Calibration line pattern. (B) Sample micrographs cut with speed 20% and power 8%. (C) Channel widths obtained with different combinations of speed and power settings. (D) Channel depths obtained with different combinations of speed and power settings. (E) Width to height aspect ratios of channels obtained with different combinations of speed and power settings. (F) Surface profile of a channel machined with 8% power and 60% speed.

The cross-section of channels created with vector cuts had a Gaussian shape due to the Gaussian shape of the laser beam. When the PMMA was ablated by the laser, its temperature rose at the irradiated spot. The PMMA then both vaporized and melted leaving molten polymer that was removed from the void created by the laser by the gas pressure of the evaporated PMMA. The molten polymer moved toward the rim of the channel where it solidified when it encountered cooler air thereby creating bulges at the edge of the channels (Fig 8F). These bulges can be problematic when sealing the channels since they are not uniform and can affect the conformational bonding of the sealing layer to the substrate. Methods for reducing these bulges and the overall surface roughness of PMMA are discussed in Section 5.4.

3.4 Raster Engraving Characterization

Raster cuts can be used to fabricate microchannels with higher aspect ratios by scanning the laser across the material similar to an inkjet printer. They can also be used to create other features such as chambers and cavities. During raster engraving, the substrate is ablated, and the thermal energy will diffuse to its surroundings. The area to be ablated in the next pass is then pre-heated by the heat from the previous pass making it easier to melt and vaporize. This causes the depths of rastered features to be slightly deeper than depths created with single-pass, vector cuts[23].

Though they are slightly deeper than vector cuts, wider microchannels can be created with rastered engravings while minimally increasing depth. Raster engravings are recognized by increasing the lineweights of features in a CAD drawing to above 0 mm. The pattern in Fig. 9A was raster cut with different lineweights increasing from 0.05 to 0.6 mm with a power of 30% and a speed of 40% in 3.1 mm thick PMMA. The widths and depths were measured using a light microscope and the widths were compared to their set lineweights defined in the CAD file. Overall, the widths did not vastly differ from their set lineweights and higher aspect ratios were achieved (Fig. 9C). However, the surface roughness of the channel after laser processing was very high and would need more processing to be reduced (Fig. 9D and E).
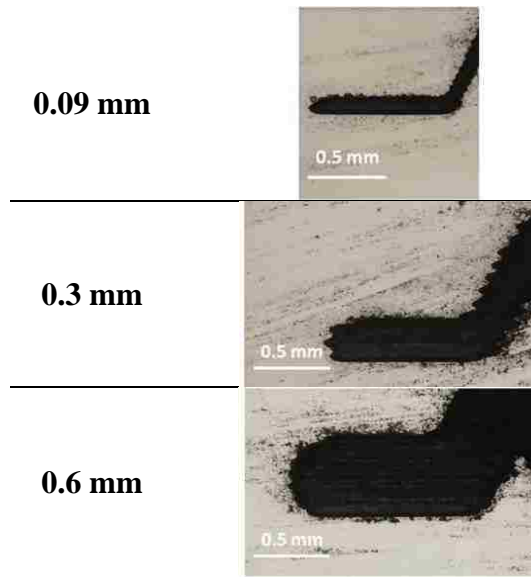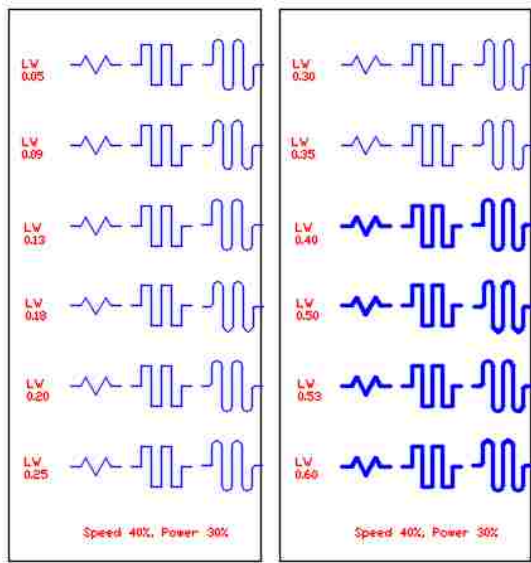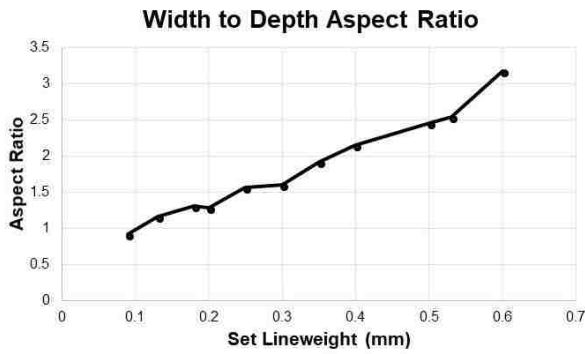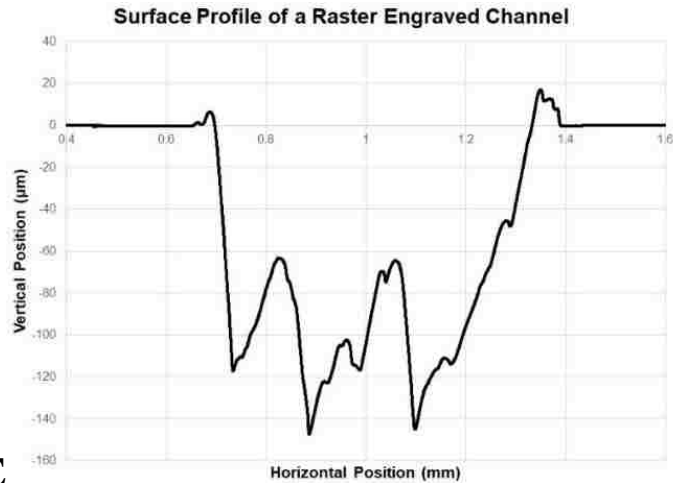
Figure 9: Raster engraving characterization with VLS 3.60. (A) Calibration line pattern with lineweights varying from 0.05 to 0.6 mm cut with speed 40% and power 30%. (B) Sample micrographs of rastered design with varying lineweights. (C) Width to height aspect ratios of channels obtained with different lineweights (D) Cross-section of a laser machined channel with 0.6 mm lineweight. (E) Surface profile of a channel with 0.6 mm lineweight.

14

3.5 Conclusions

The VLS 3.60 was shown to be able to produce small channel sizes using vector engravings that had a Gaussian shape. However, vector engravings yielded low aspect ratios and the engraved channels exhibited bulges around the channel rims that can make sealing the channels difficult. These bulges can be reduced by controlled exposure to solvents. Rastered engravings produced higher aspect ratio features. Their surface profiles, however, were extremely rough and would also need to be exposed to solvents for surface roughness reduction.

4. Improving the Manufacturability of a Personalized Drug Testing Microfluidic Platform

4.1 Introduction

Several studies have previously used laser micromachining as a method to produce microfluidic devices. Keramas et al. developed a multiplex DNA microarray system that consisted of four layers of PMMA, PDMS, and glass. Using a laser cutter, channels, holes, and cavities were machined into the PMMA to create a microfluidic structure of delivery channels that led to 32 reaction chambers with DNA probes hybridized to a glass slide[24]. Qi et al. developed a continuous-flow PCR (polymerase chain reaction) microfluidic device using PMMA and a CO_2 laser source[25]. The device had a network of serpentine channels to facilitate 20 amplification cycles. An oxygen gradient generator biochip was developed by Skolimoski et al. where a cell culture chamber and channel network to be filled with oxygen scavenging liquid were machined with a CO_2 laser into PMMA[26].

Though these devices provide important functions such as the study of DNA and cells, there are few microfluidic devices that address intact tissues. Furthermore, there are no such devices that are machined using lasers. Chang et al. have developed a personalized microfluidic device that facilitates live tissue slice cultures and has a channel network that delivers drug solutions to the slices[27]. The device, herein called OncoSlice, was meant to allow for high-throughput drug delivery to cancer slices to identify the most optimal and beneficial therapies for individual patients. It can also be used for toxicology studies. The device was composed of four PDMS layers that formed a channel network and a polystyrene (PS) 96-well plate with the centermost 16 wells cut out which formed a tissue culture chamber (Fig. 10A). The remaining 80 wells were filled with drugs, and a syringe pump controlled the flow of the fluids by inducing negative pressure. This pulled the fluids through 80 delivery channels that delivered drugs to 80 "roofless" channels, otherwise known as drug lanes, in the tissue culture chamber. Atop these lanes sat a porous polytetrafluoroethylene (PTFE) membrane on which tissue was placed and which sealed the open, roofless drug lanes. As the fluids flowed through the roofless lanes, they diffused through the PTFE membrane and into the tissue (Fig. 10B). The lanes were connected to a single outlet by a binary network of channels.

The channel network was formed by aligning and bonding together using oxygen plasma treatment the PDMS layers. These layers were then bonded to the well plate. This process was extremely labor intensive and required a high level of expertise since all the PDMS layers had to be perfectly aligned for all 80 channels to function correctly. Consequently, manufacturing of this device saw a high failure rate and was rarely reproducible by other skilled personnel. The total fabrication time was approximately four days. To reduce costs and fabrication time and to simplify the fabrication methods the device was transitioned from conventional fabrication using PDMS soft lithography to laser micromachining of PMMA. The development of the fabrication protocol based on laser micromachining is discussed in this section.

16
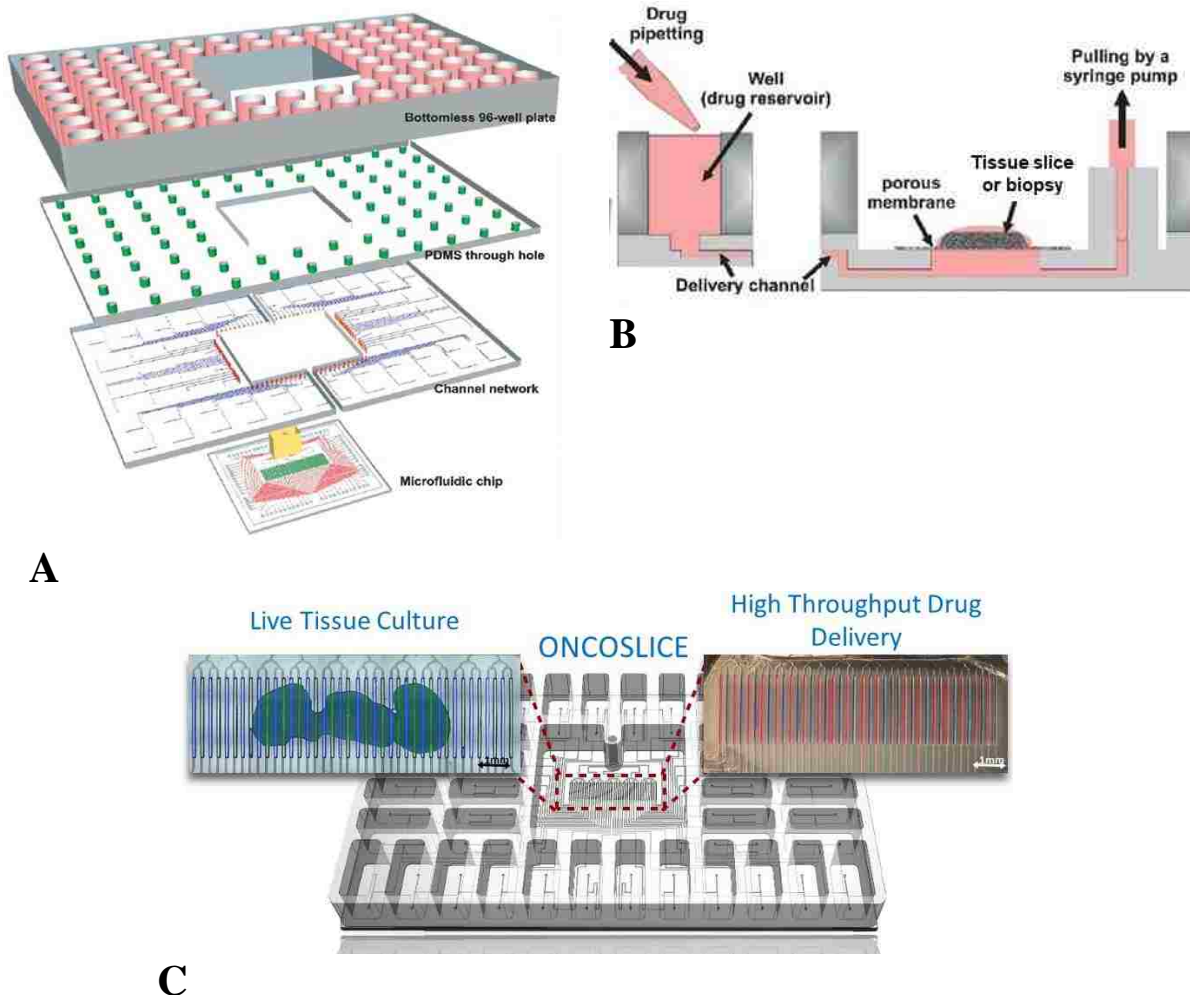
Figure 10: A personalized drug testing microfluidic platform called OncoSlice that integrates live tissue slice cultures with a multi-well platform that allows for exposing the slices to multiple compounds simultaneously. (A) Previous device design that was composed of four PDMS layers bonded together to a modified PS 96-well plate - image reproduced from Ref. 27 with permission from The Royal Society of Chemistry. (B) Device operation where a syringe pump controls the flow rate of fluid streams in the channel network and where fluids diffuse up through a porous PTFE membrane and to the tissue - image reproduced from Ref. 27 with permission from The Royal Society of Chemistry. (C) Laser micromachined OncoSlice device made only of PMMA.

4.2 Current Device Fabrication Protocol

Our device fabrication protocol can be easily replicated in other labs given that they have similar tools and materials as described in this research. Some optimization may be needed but the process outlined in this research can be used as a guiding framework.

The current OncoSlice device consists of a 40-well plate with an integrated channel network layer fabricated by laser micromachining PMMA substrates and solvent bonding them together. The device was composed of three layers: a PMMA bottomless 40-well plate, a PMMA channel network layer, and a PMMA sealing layer (Fig. 11). This is a reduction in the number of layers compared to the PDMS-based device and all the layers are made of a single material instead of PDMS and PS. An overview of the fabrication protocol is displayed in Fig. 12.

The bottomless PMMA plate has wells that each can hold a maximum volume of 1.6 mL. This is eight times more volume that can be held in a well than a PS 96-well plate. This increases convenience because the device can be run for longer before the wells almost deplete and must be refilled with drug solutions to extend testing on tissue slices.

The plate was created by laser cutting holes into a 19 mm thick PMMA sheet. 40 rectangular shaped holes (each 6 x 16 mm) that form wells of the device were cut along with a square hole in the center of the plate that formed the tissue culture chamber area. The plate itself was then cut out of the sheet. Warping becomes an issue when cutting the plate due to a high amount of heat being applied to the PMMA. Consequently, the plate was placed for 20 minutes in a heat press (Carver 4386 Model CH) set near the glass transition temperature of PMMA and then cooled for 20 minutes while being pressed to return the plate to a flat state.

The channel network layer was created by engraving channels onto a 300 μm thick PMMA sheet. The network was designed such that the channels leading to the roofless parallel channels in the center of the device have the same length and therefore the same fluidic resistance. The speed and power settings of the laser were optimized to yield specific channel dimensions (Fig. 15B). The roofless parallel drug lanes were created by slowly etching away PMMA using multiple passes with the laser at a low power and fast speed. This method yielded sharper, cleaner cuts compared to single passes with a higher power and slower speed.

The sealing layer was meant to provide a "floor" for the channels since they are open when the channel network layer is engraved. This layer was a thin 125 μm PMMA film that was laser cut to have the same dimensions as the outline of the channel network layer.

The channel network layer was sealed using a chloroform vapor treatment and heat press bonding method. The chloroform vapor treatment was performed by placing a glass container into a water

18

bath. Four stainless steel hose clamps (10 mm in height) were placed in the glass container and were used as stand offs. The glass container was firstly filled with chloroform. A plastic lid was loosely placed on top of the glass container and the vapor in the container equilibrated for approximately four minutes. After, the channel network layer was attached to an adhesive to prevent it from falling into the chloroform. The adhesive and the channel network layer were then placed on top of the stand offs. With the lid closed, the layer was exposed to the chloroform for 4 minutes after which it was removed. The sealing layer was then attached to the adhesive, placed on top of the stand offs, and exposed to the chloroform for 2 minutes. After exposure to the chloroform, both layers were slightly adhesive due to dissolution. The sealing layer and the channel network layer were then pressed together by hand to prevent the two layers from sliding against each other and misaligning in the heat press. The two layers were then sandwiched between two blank PDMS layers and placed in a heat press whose platens have been preheated to 60˚C. The layers were pressed together for 10 minutes. The PDMS layers serve to distribute pressure more evenly across the layers and reduce the formation of air pockets.

Prior to bonding of the channel network layer to the plate, the side of the plate to be bonded was exposed to chloroform for 30 minutes to reduce surface roughness. The setup for this chloroform vapor treatment was the same as the setup for the treatment of the channel and sealing layers. While this treatment was being performed a circle 1.5 mm in diameter was punched out of a 125 μm thick PDMS film and placed over the outlet of the channel network layer to protect it from exposure to methylene chloride, a solvent that is later used to bond the plate and channel network layer together. After the plate was treated, it was dried by letting it sit in open air for 10 minutes. The side of the plate to be bonded was then immersed in methylene chloride for 15 seconds. The channel network layer was then aligned by eye to the plate and pressed by hand onto the plate. The plate and the channel network layer were then sandwiched by two PDMS slabs one of which has a 500 μm thick piece of PMMA attached to it to add more rigidity to the assembly. The whole assembly was pressed together at approximately 200 psi for 5 minutes in a hydraulic press.
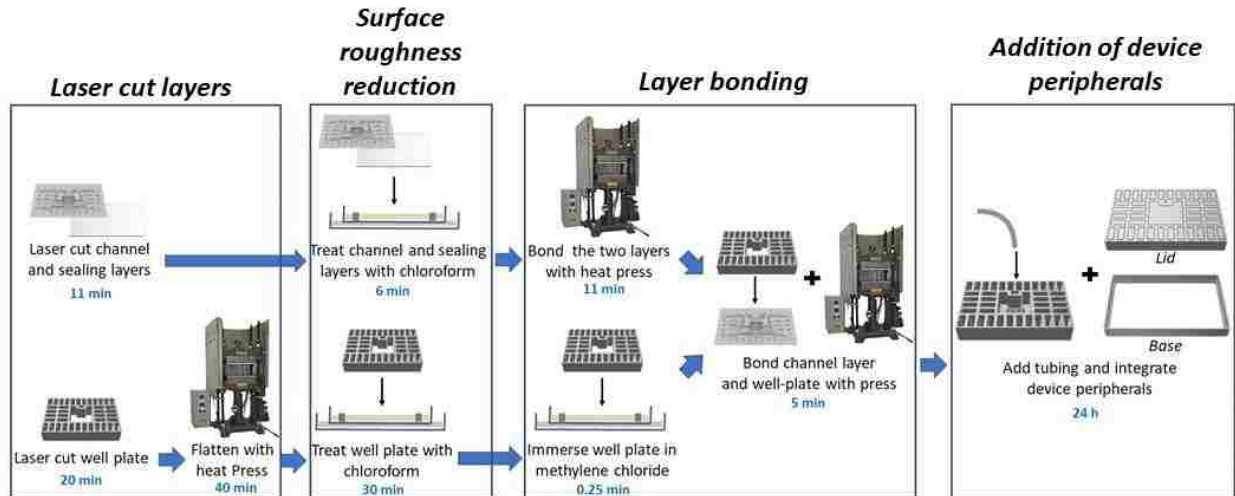
Figure 12: Overview of the OncoSlice device fabrication protocol. All components of the device were firstly cut or engraved with a laser cutter. The channel network layer was formed by treating the PMMA piece with the engraved channels and the sealing layer with chloroform and heat pressing the two layers together. The well plate was prepared for bonding with the channel network layer by flattening it, treating it with chloroform, and immersing it in methylene chloride. The channel network layer and the well plate were then bonded together with a hydraulic press. Tubing was added to outlet to interface with a syringe pump and a lid and base were added to the device.

Silicon tubing with an inner diameter of 0.76 mm and an outer diameter of 2.5 mm was cut into 63.5 mm in length and was inserted into a hole in the plate that connects to the channel network layer outlet. The plate was designed such that a well was formed around the outlet hole for tubing at the top of the plate. After the tubing was inserted, the well was filled with super glue to secure the tubing into place and to provide an air tight seal.

A lid mimicking a petri dish lid and a base that allows the device to fit onto imaging platforms were formed by laser cutting PMMA layers and bonding them together using a double-sided adhesive. They were then attached to the device.

4.2.1 Fabrication Time

The process manufacturing time to produce one PDMS-based device was about four days considering all the fabrication of the master molds and the PDMS molding, curing, and bonding. For our current fabrication protocol, the process manufacturing time is approximately two hours after totaling all the steps outlined in Table 1. This is a significant reduction in fabrication time and with the ease of our protocol, costs can be decreased, and users do not high expertise in microfluidic device fabrication to reproduce this device. Several devices can be fabricated in one day and would be ready for use the next day.

Step	Time (min)
Laser Cutting	
Laser Cut Channel Network Layer and Well Plate	27
Laser Cut Lid and Base	5
Cleaning with IPA	5
Channel Network Layer Assembly	
Channel Network Layer and Sealing Layer Chloroform Treatment	6
Hand Bond and Heat Press	11
PMMA Well Plate Assembly	
Flatten	40
Chloroform Treatment and Methylene Chloride Treatment	30.25
Hand Bond and Press	7
Device Accessories and Surface Modifications	
Outlet Insertion and Lid and Base Assembly	7
Plasma Treatment	5
Total	*143.25*

4.3 Incorporation of Digital Manufacturing Techniques for a More High-throughput Fabrication Protocol

4.3.1 Channel Network Layer Architecture Iterations

The design of the channel network layer was created by matching hydraulic resistances for each delivery channel so that diffusion of drug solutions into the membrane and tissue samples were equal. According to the Hagen-Poiseuille Law, volumetric flow rates will be equal in channels that have the same hydraulic resistance and experience the same pressure drop. Equal volumetric flow rates lead to equal rates of diffusion of fluids from the drug lanes to a tissue sample. Hydraulic resistances within a circular microchannel are proportional to the cross-sectional area and length of the microchannel and can be expressed as

$$R_H = \frac{8\eta L}{\pi R^4}$$

Equation 1. Hydraulic resistance for a circular channel

21

where η is the viscosity of the fluid, L is the length of the channel, and R is the radius of the circular channel. For a rectangular shaped channel such as those in PMDS microfluidic devices, the hydraulic resistance can be expressed as

$$R_H = \frac{12\eta L}{wh^3}$$

Equation 2. Hydraulic resistance for a rectangular channel ($h/w \ll 1$)

where w is the width of the channel and h is the height of the channel. Note that equation 2 applies only to channels with high aspect ratios ($h/w \ll 1$). For rectangular-shaped channels, the height, width, and length can be manipulated to match hydraulic resistances of other channels.

Prior to the current channel network layer architecture used in the device, there were two iterations that preceded it. The first and second designs were primarily used in the fabrication of PDMS-based devices using soft lithography (Fig. 13A). The height of the microchannels was kept constant, while the widths and lengths were adjusted to achieve equal hydraulic resistances. In the second redesign of the channel network layer, the number of inlet channels were reduced from 80 to 40 to allow for bigger features and therefore wider alignment tolerances (Fig. 13B). The height was again kept constant and the lengths and widths were adjusted to achieve equal hydraulic resistances.

In the case of transitioning device fabrication to a laser micromachined based platform, only the lengths of the channels can be adjusted since it is difficult to adjust the width of a vector engraved microchannel while keeping its height constant (Fig. 13C). The channel network layer was redesigned by measuring the length of the microchannel that has the furthest inlet from the drug lanes in the tissue culture chamber. The lengths of all the other channels were adjusted to match this length by the addition of serpentine features. It was observed that the dimensions of curves engraved with the laser cutter were different than linear engravings. To account for this, each delivery channel was designed to not only have the same length but also the same number of 90 degree turns. The laser power and speed settings were set to be constant for each channel so that the cross-sectional area of each channel was the same. With the same length and the assumption of the same constant cross-sectional area, it was assumed that the flow rates in each channel would be equal.

A

B

23
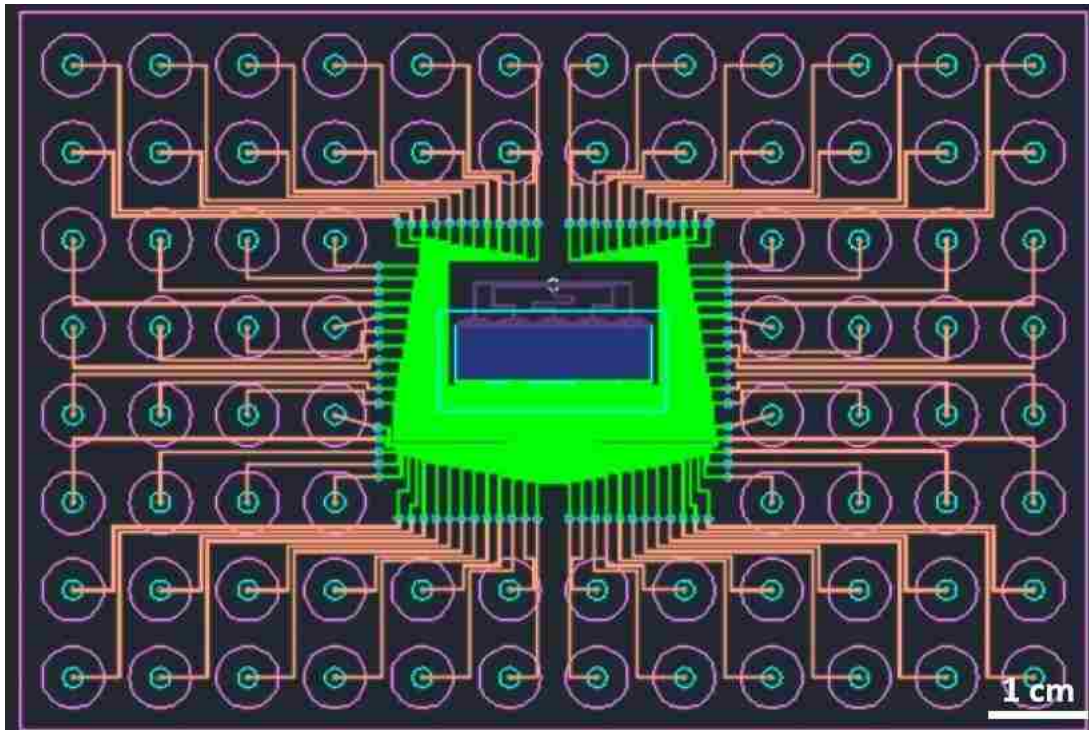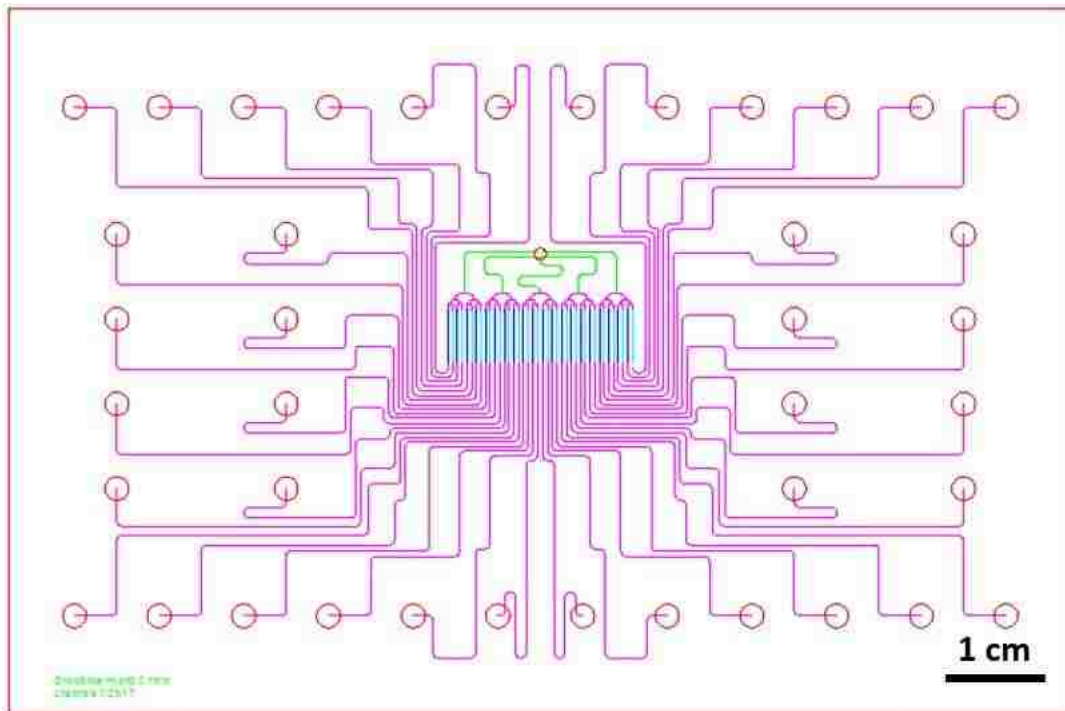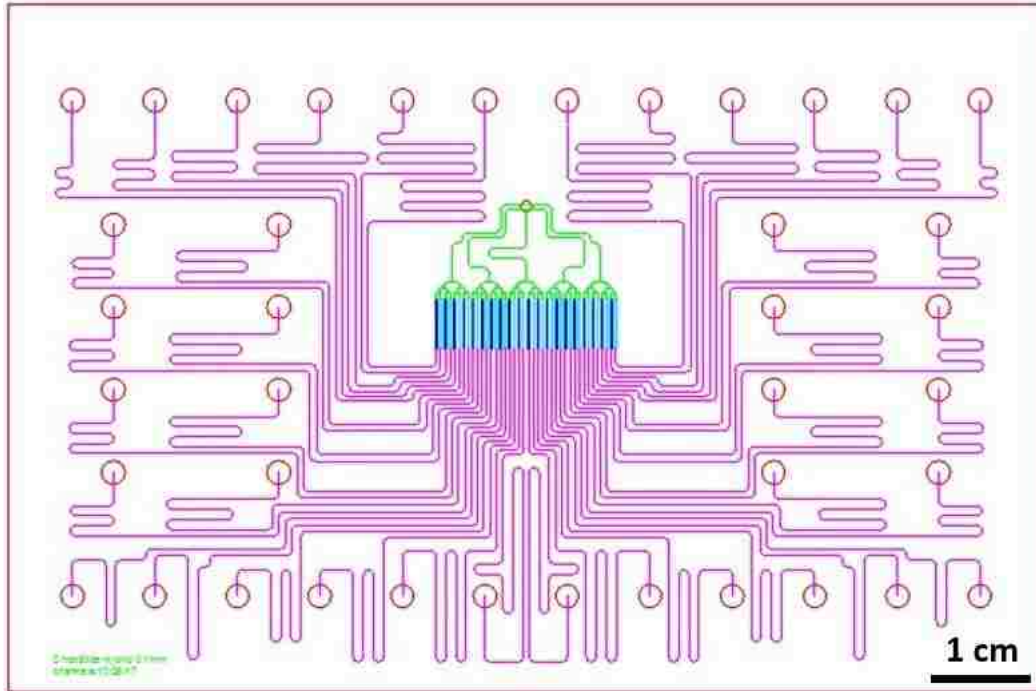
C

Figure 13: Channel network layer design iterations. (A) Initial design for the PDMS-based OncoSlice device. The heights of the channels were kept constant while the widths and depths were adjusted for equal hydraulic resistances. (B) Second design for the PDMS-based OncoSlice device. The number of channels was reduced from 80 to 40 and the heights of the channels were kept constant while the widths and depths were adjusted for equal hydraulic resistances. (C) Third design for the laser micromachined OncoSlice device. Heights and widths of channels were constant when formed by laser engraving, so lengths were adjusted to match the length of the inlet furthest from the lanes.

In the final design iteration, the length of each channel was 85.2 mm and the length of each drug lane was 5.43 mm. The width of each drug lane was set to be 100 μm, though the actual dimensions depended on the laser cutter power and speed settings (Fig. 15). The distance between each drug lane was 500 μm from center to center.

4.3.2 Fabrication Using Laser Micromachining

4.3.2.1 Laser Settings Optimization
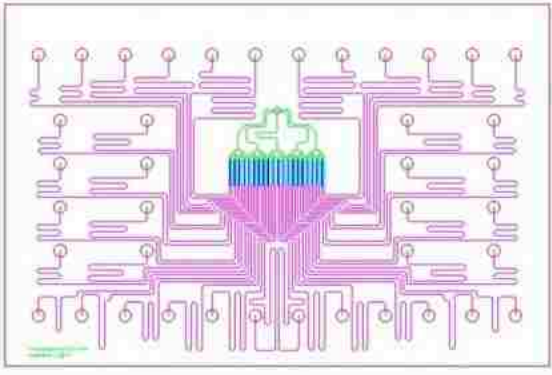
The main components of the channel network layer are the channels that deliver fluids from the wells to the tissue culture chamber, the drug lanes in the tissue culture chamber, the binary network of channels that connect the outflow of the lanes to the singular outlet, and holes for the inlets and the outlet.

Optimization of the laser settings for the delivery channels and the binary network was done by choosing an appropriate power setting and then adjusting speed settings such that the laser did not cut through the plastic in one pass. The chosen setting for the delivery channels was a power of 8% and a speed of 40%. The chosen setting for the binary network was a power of 8% and a speed of 35%. The binary network had a lower speed setting which yields deeper and wider channels. This was to reduce resistance in these channels. The syringe pump does not allow the device to be run longer than 28 hours when set at 2 ml/hour, so fluid in the syringe must be emptied and wells

24

refilled with drugs for longer use of the device. Emptying the syringe requires disconnection of the pump from the device. During this time of disconnection, backflow of fluids occurs, so lower resistance in the outlet binary network was needed to reduce backflow of drugs into the lanes and into tissue samples. The settings for cutting the channel network are in Table 2.

Optimization of the open lanes was done similarly to the channel features. An appropriate power was chosen, and the speed adjusted such that through-cuts were made in the plastic for each lane. However, this approach usually led to warping of the walls of the lanes. Consequently, a three-pass approach with a lower power and higher speed was taken to cut the lanes. Applying three passes to cut through the PMMA was a slower, more controlled approach to creating the lanes which are only several hundred microns apart. This also greatly reduced stress on the walls of the lanes as they were being formed and therefore caused no warping. This also reduced polymer reflow that would otherwise clog the lanes. The optimized settings for the lanes were three passes each at a power of 10% and a speed of 40%.

Table 2: Channel Network Layer Laser Cutting Settings

CAD Design	Color in CAD Design	Layer Feature	Power (%)	Speed (%)	Number of Passes
1 cm	Magenta	Delivery Channels	8	40	1
	Green	Binaries	8	35	1
	Cyan and Blue	Open Drug Lanes	10	40	3
	Red	Inlets, outlets, layer outline	15	15	1

4.3.2.2 500 μm Thick Channel Network Layer

The lanes for the 500 μm thick channel network layer had a trapezoidal cross-sectional shape rather than an ideal rectangular shape (Fig. 14A). This was because the laser was set to focus on the top surface of the PMMA. If a material is thick, the laser will be out of focus as it cuts in a deeper plane in the z-direction and the dimension of the cut in this plane will be different than on the top surface. The width of the lane that contacts the PTFE membrane was smaller than the width that contacts the PMMA sealing layer. For this reason, we decided to use a 300 μm thick PMMA sheet for our channel network layer to allow for less discrepancy between the widths of the top and bottom of the lanes. Increased flexibility of 300 μm thick PMMA also allowed the channel network layer to conform better to the 40-well plate.
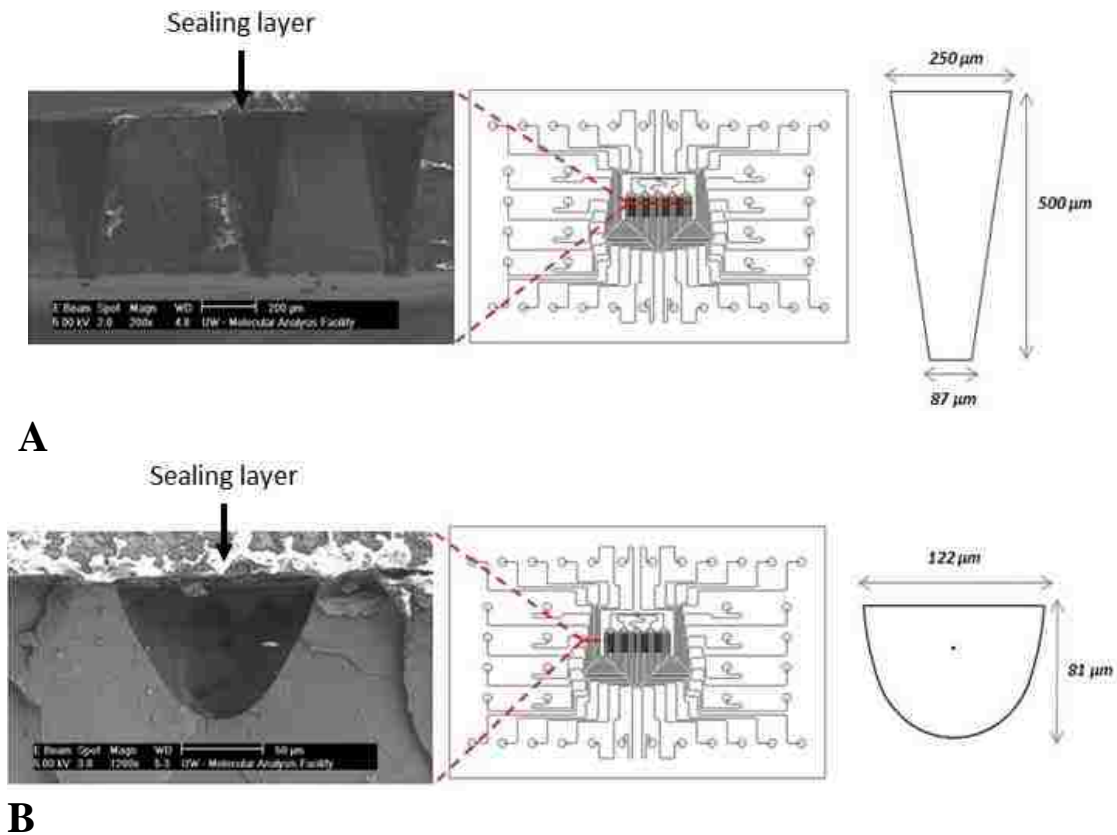
Figure 14: Scanning electron micrographs of 500 µm thick channel network layer. (A) Cross-section of the open drug lanes. Laser cutting yielded a trapezoidal shape where the opening that faces the membrane and tissue had a width of about 90 µm. (B) Cross-section of the delivery channels. Laser cutting yielded a Gaussian shape with a base width of about 120 µm and a height of about 80 µm.

4.3.2.3 300 µm Thick Channel Network Layer

The widths of the top and bottom of the lanes differed by 163 µm in the 500 µm thick channel network layer. With the 300 µm thick channel network layer, this was reduced to 100 µm (Fig. 15A).

Since the focus of the laser did not change with the difference in thicknesses of the PMMA substrates, there was little change in the cross-sectional shape of the channels. The dimensions of the delivery channels did not change significantly between the 500 and 300 µm thick PMMA. The width of the channel was 130 µm and the depth was 75 µm.

A

B
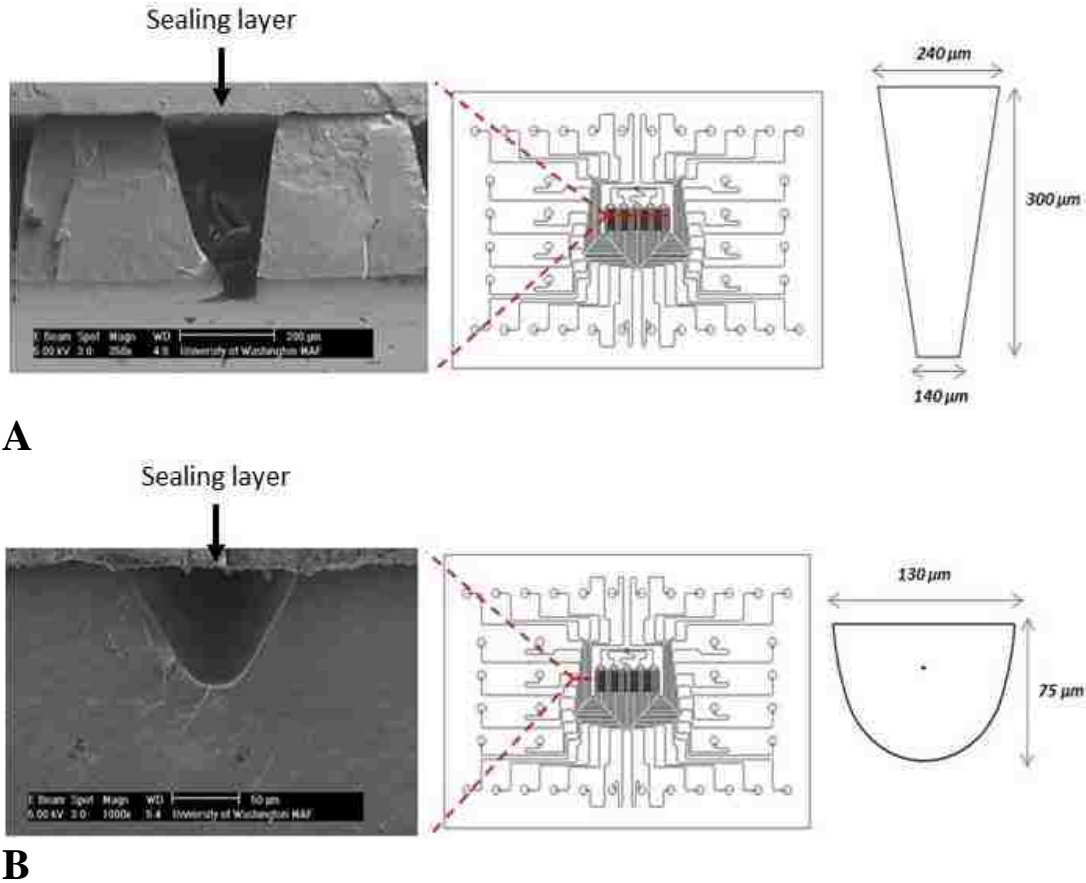
Figure 15: Scanning electron micrographs of 300 μm thick channel network layer. (A) Cross-section of the open drug lanes. Laser cutting yielded a trapezoidal shape where the opening that faces the membrane and tissue had a width of about 140 μm. (B) Cross-section of the delivery channels. Laser cutting yielded a Gaussian shape with a base width of about 130 μm and a curve height of about 75 μm.

This thickness of the channel network layer provided enough flexibility to be bonded to the 40-well plate and more uniformity in the channel features. Additionally, the 300 μm thick PMMA channel network layer allowed the device to be operated for longer uninterrupted by the need to refill the wells with solutions. The cross-sectional area of the lanes was smaller than the 500 μm thick PMMA. For the same volumetric flow rate set on the syringe pump, this causes the fluid velocity to increase. This was dictated by Equation 3

$$Q = Av$$

Equation 3. Volumetric Flow Rate

where Q is the volumetric flow rate, A is the cross-sectional area of a channel, and v is the fluid velocity. Fluid velocity determines lateral diffusion of drugs in the porous membrane and in the tissue samples. An appropriate volumetric flow rate set on the syringe pump must be chosen to limit lateral diffusion and drug cross-talk. Therefore, to achieve the same fluid velocities between the 300 and 500 μm thick PMMA, the flow rate set on the syringe can be lowered and the device can be operated for longer when using the 300 μm thick PMMA. Assessment of lateral diffusion

27

at different flow rates to find a minimum flow rate that prevents diffusion is described in Section 4.7.3.

4.3.2.4 PMMA Well Plate

The PMMA plate could be made in two different ways. One consists of bonding three 6.35 mm thick plates together. The VLS 3.60 was used to cut these plates. Another way is to cut a single 19.05 mm thick plate. This was more ideal since this required less post-processing steps, however, this required another laser system with more power.

Orthogonal View

Front Perspective Views
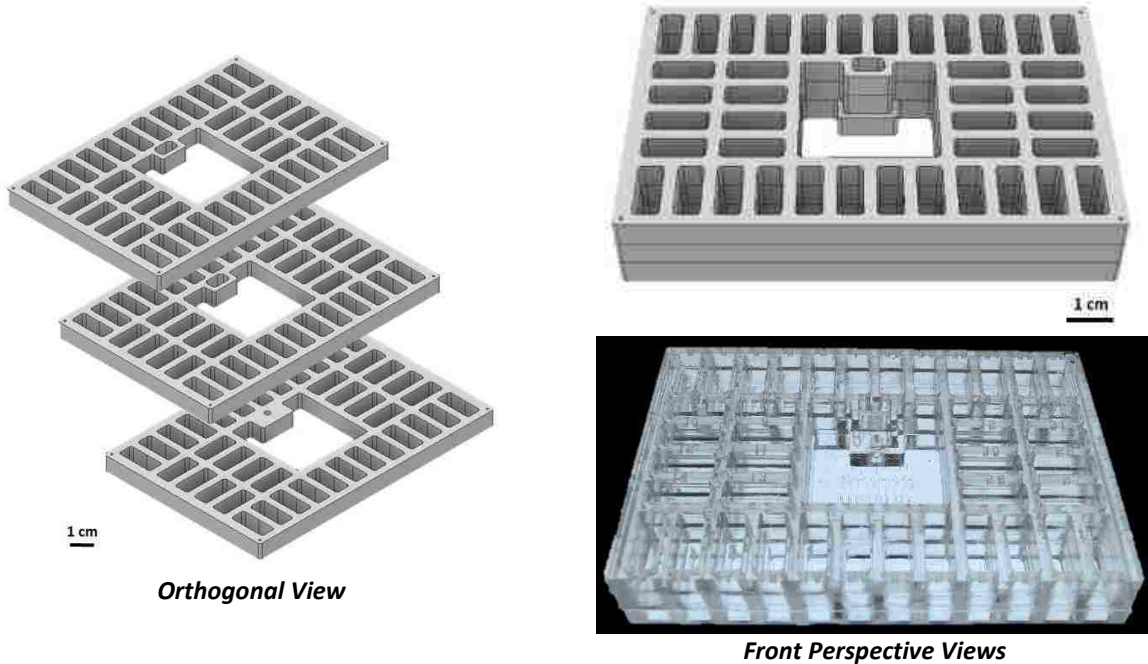
Figure 16: Well plate made from three bonded 6.35 mm thick PMMA layers

The VLS 3.60 laser system can cut 6.35 mm thick PMMA sheets in a single pass. This required a power of 100% and a speed of 1.5%. A 19.05 mm thick PMMA well plate composed of three separate plates required cutting each plate and bonding them together (Fig. 16). The dimensions of the wells in each of the three plates were the same. In terms of the outlet of the plate, however, the bottommost plate differed from the other two plates. The outlet requires tubing to be pushed through a hole in the plate and sealed tight. This was achieved by cutting a hole with the same diameter as the tubing in the bottommost plate. The tubing connected the outlet of the channel network layer to the syringe pump. The other two plates had a rectangular shaped hole that was larger than the hole for the tubing. This was done so that the top two plates formed a well around the tubing (Fig. 30) which was then filled with super glue to secure the tubing in place and form an air tight seal that would have otherwise interfered with the suction mechanism of the syringe pump.

28
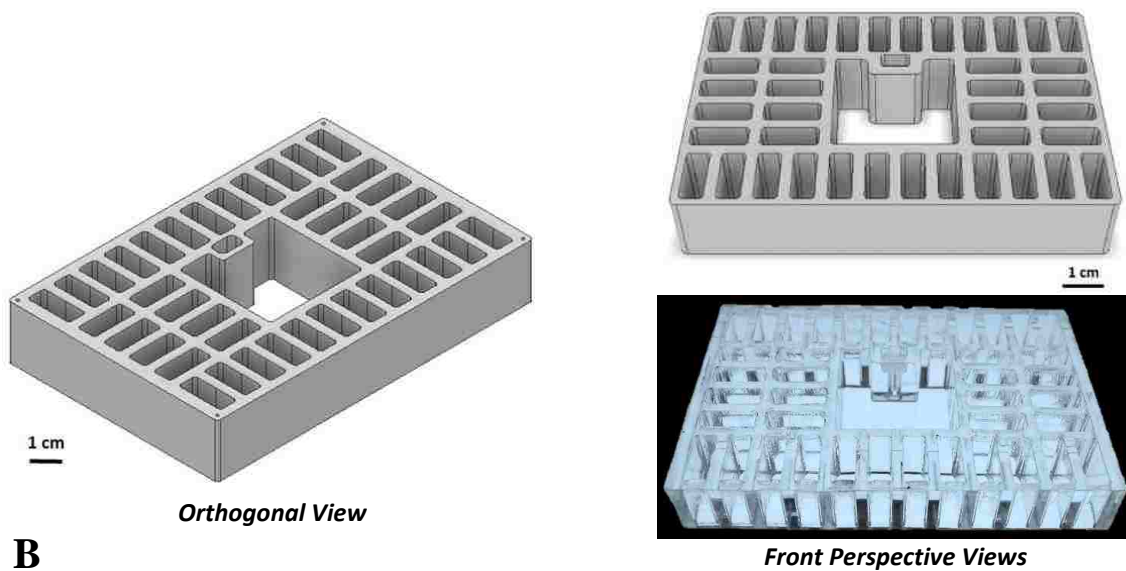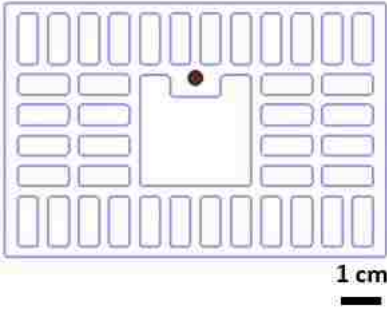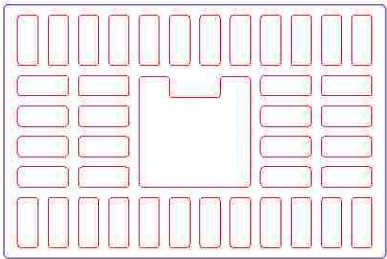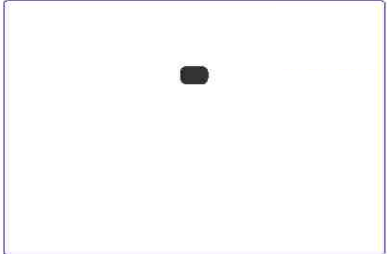
Figure 17: Well plate made from a single layer. (A) ILS 12.150D laser cutting System. (B) CAD models and picture of a single-layer laser cut well plate.

The ILS 12.150D laser system from ULS has a maximum power of 150 W and can cut 19.05 mm thick PMMA sheets if done with multiple passes. Using this system, a 19.05 mm thick PMMA substrate was placed in the cutting bed with the side of the plate to be bonded to the channel network layer (i.e. the bottom side of the plate) facing up. The hole for the outlet tubing was first cut along with a shallow raster engraving that widened the outlet hole. The plate and the channel network layer are bonded with a solvent. The widening of the outlet in the plate with a rastered engraving prevents the solvent from coming into contact with the outlet of the channel network layer. If the solvent encounters the binary channels in the outlet of the channel network layer and occludes them, then the device will not function as intended. Cutting the plate with the bottom face up ensured that the dimensions of the hole for the outlet match the dimensions set in the CAD file since the laser goes out of focus the deeper it cuts into a material. The dimensions of the plate on the top side did not match the dimensions set in the CAD file since the laser was out of focus. The features on this side are less critical, however, and therefore have more tolerance. After the outlet hole for tubing and the wells were cut, the plate was flipped over, and the well to be filled with

super glue was created using a rastered engraving. The order of which features were cut first for the well plate along with the laser settings are outlined in Table 3 and the finished part is shown in Fig. 17.

Table 3: Well Plate Laser Cutting Settings

CAD Design	Pass Number	Color in CAD	Purpose	Power (%)	Speed (%)
Create Hole for Tubing 1 cm	1	Black	Raster Engraving	50	28
		Red	Vector Cut	100	0.8
		Blue	Alignment	0	0
Cut Wells and Outline 	1	Red	Vector Cut	100	4
	2	Red	Vector Cut	100	2
	3	Red	Vector Cut	100	0.8
	4	Blue	Vector Cut	100	4
	5	Blue	Vector Cut	100	2
	6	Blue	Vector Cut	100	0.8
Create Well for Sealing Outlet 	1	Black	Raster Engraving	50	5
		Blue	Alignment	0	0

4.3.2.5 Device Accessories

Our device can be kept within a large petri dish with a hole drilled within the lid to allow the tubing to connect to the syringe pump. However, a custom-built lid can reduce the overall size of the device when in use. We developed a lid that has similar functional features as a PS 96-well plate lid which mainly consists of small supports and an overhang. The supports elevate the top surface of the lid above the dish and form small slits for air to pass through and circulate in the device.

The overhang serves to force air to come down and then back up to enter the dish thereby filtering out dust, heavy particles, and other contaminants (Fig. 18B). To achieve these features in a PMMA lid, we cut three layers of PMMA of varying thicknesses and bonded them together with double-sided tape. The top layer had numbers engraved on the top to denote each well and a hole cut through to connect the outlet tubing to the syringe pump. The middle layer had the shape of a rectangular frame and on each of its corners were four offsets that contact the device on its four corners (Fig. 18C). The offsets elevated the top layer of the lid above the device and created slits for air similar to 96-well plate lids. Attached to the bottom of the middle layer was a thicker piece of PMMA that also had the shape of a rectangular frame minus the offsets. This bottom layer of the lid served as the overhang that filtered out dust and contaminants. The settings for cutting these layers are outlined in Table 4.

A

B

C

D
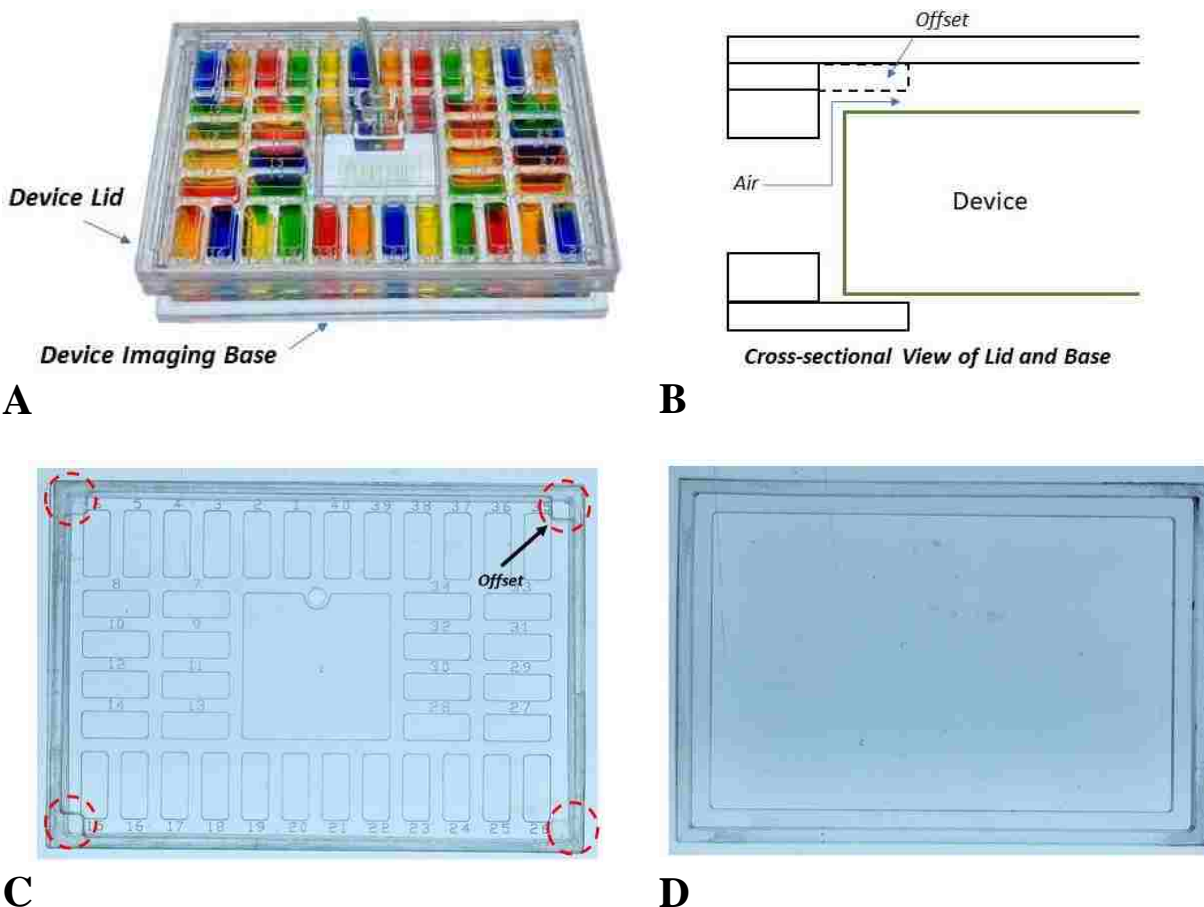
Figure 18: OncoSlice device accessories. (A) Micrograph showing device with a lid and imaging base. (B) Cross-section of the device with accessories. The lid filters out contaminants similar to a lid for a 96-well plate and the base allows the device to fit onto fluorescence microscope stages. (C) Top view of the device lid. (D) Top view of the device imaging base.

A standard 96-well plate has a base that elevates the wells. Additionally, most microscopy imaging systems have stages to accommodate 96-well plates. Our device alone could not fit onto most imaging stages. It was too small and would fall through the stage. Consequently, we created our own base to allow our device to be imaged with our microscopy system. It consisted of two PMMA frames bonded together (Fig. 18D). The bottom frame had an outer dimension of 121 x 83 mm and

an inner dimension of 106 x 68 mm. The top frame had an outer dimension of 121 x 83 mm and an inner dimension of 115 x 77 mm. The bottom frame has a smaller inner dimension to provide support for the device and elevate it so that the channel network layer does not contact the surface on which the base sits while the top frame serves to secure the device in place and provide a tight fit. The settings for cutting these layers are outlined in Table 5.

Table 4: Device Lid Laser Cutting Settings
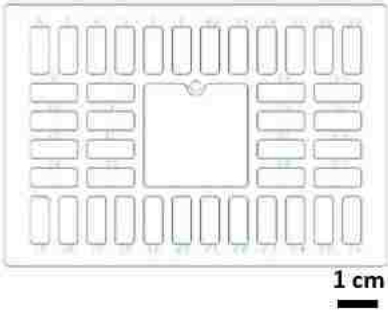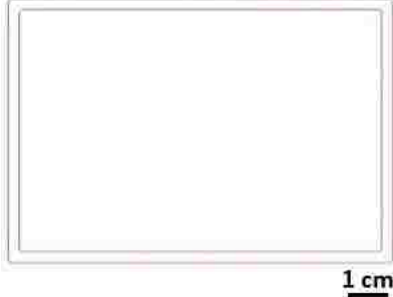
CAD Design	PMMA Thickness (mm)	Color in CAD	Purpose	Power (%)	Speed (%)
Top Layer 1 cm	3.18	Red	Vector Cut	100	4
		Green	Vector Engraving	80	20
		Blue	Vector Engraving	80	20
Middle Layer	3.18	Red	Vector Cut	100	4
Bottom Layer	6.35	Red	Vector Cut	100	1.5

Table 5: Device Imaging Base Laser Cutting Settings

CAD Design	PMMA Thickness	Color in CAD	Purpose	Power (%)	Speed (%)
Top Layer	6.35	Red	Vector Cut	100	1.5
Bottom Layer	3.18	Red	Vector Cut	100	4

4.4 Post-processing of Laser Micromachined Parts

4.4.1 IPA Sonication

The VLS 3.60 is equipped with a lateral gas assist that blows air in the areas where the laser cuts. This removes PMMA debris as the laser moves across the plastic. However, some debris remains after cutting and engraving despite the gas assist. As such, all PMMA pieces cut with a laser were rinsed with DI water, sonicated in isopropyl alcohol (IPA) for 2 minutes, rinsed with deionized (DI) water again, and dried with nitrogen. IPA efficiently removed any loose debris and burned material that may occlude channels or interfere with tissue culture experiments.
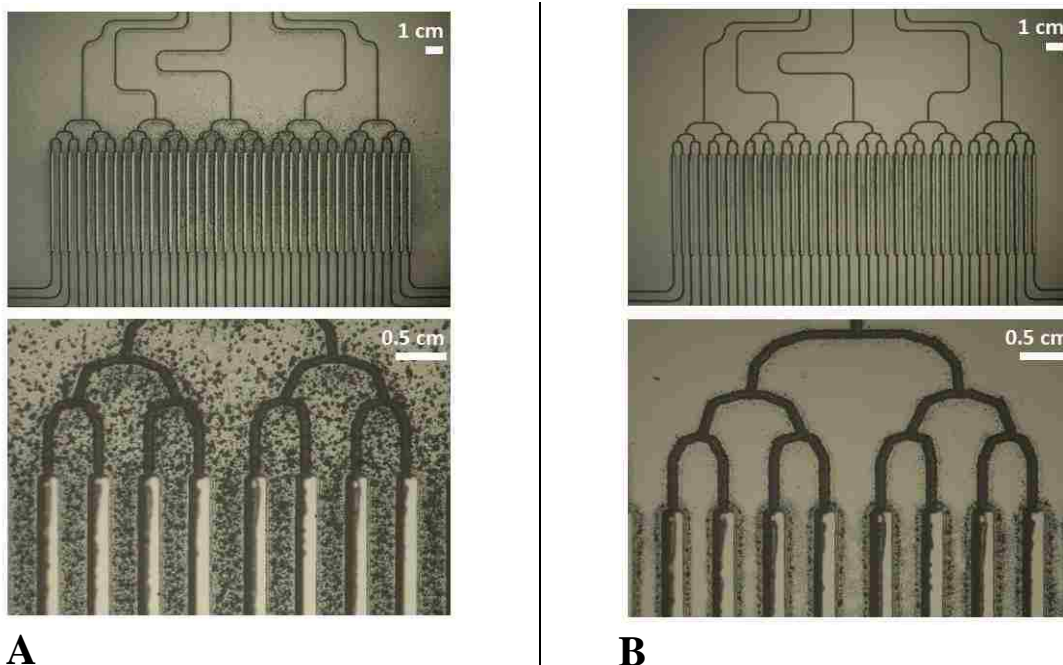
Figure 19: Cleaning channel network layers by sonicating with IPA. (A) Micrographs of a channel network layer before sonication. (B) Micrographs of a channel network layer after sonication.

4.4.2 Well Plate Flattening

Well plates cut with the ILS 12.150D became warped due to the large amount of heat applied to cut through the entire thickness of the PMMA. The thermally induced stress caused a change in shape that prevents the plate from bonding strongly to the channel network layer. To reshape the plate and create a flat bottom, the plate underwent a process call thermal annealing (Fig. 20). It was pressed in a heat press at 1000 to 1500 psi with the platens set to 110˚C. This temperature was chosen because the glass transition temperature of PMMA is between 105˚C to 115˚C and at this temperature PMMA becomes soft[20-22]. The plate remained pressed for 20 minutes after which the heater was turned off and the plate was cooled to about 45˚C using the press' cooling mechanism, which runs air over the platens. The plate was cooled while still being pressed for 20 minutes and the polymers in the substrate realigned to conform to the flat surfaces of the platens.

Warped Plate   1000-1500 psi
20 min at 110˚C
20 min cool down   **Flattened Plate**

Figure 20: Thermal annealing process to remove well plate warping

4.4.3 Chloroform Vapor Treatment

Laser micromachining left a slight bulge around the rim of the channels as the laser moved across a substrate. The bulges in the engraved channels in the channel network layer interfered with the sealing of the channel network. Consequently, Ogilvie et al. have developed a method to reduce the impact of this lip formation and reduce overall surface roughness of PMMA[20]. This method involves exposing PMMA to a solvent vapor of chloroform that induces polymer reflow of a very thin layer of PMMA on its surface and thereby removes rough features.
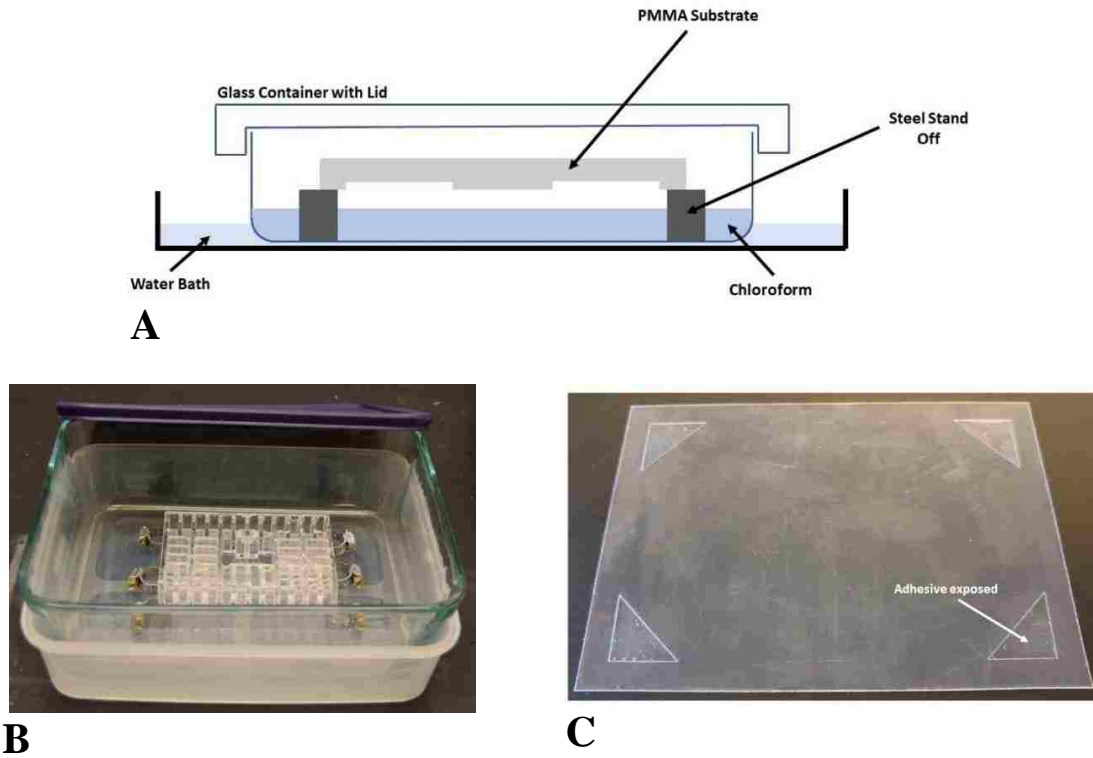
Figure 21: Chloroform treatment setup. (A) Schematic of setup. (B) Chloroform bath within a fume hood. (C) Mylar adhesive to prevent the channel network layer from falling into chloroform bath.

All chloroform treatments were performed inside a fume hood since chloroform causes carcinogenic and mutagenic effects if inhaled. The setup for chloroform treatment in the fume hood consisted of a glass container (264 x 165 x 213 mm) being placed in another container that contains room temperature water. Stainless steel hose clamps 10 mm in height were used as standoffs and were carefully placed in the glass container such that they supported the four corners of the channel network layer (Fig. 21A and B). The glass container was then filled with 60 mL of chloroform so that the distance between the top surface of the chloroform and the channel network layer was 8 mm. The lid for the glass container was put on and the chloroform vapor was left to equilibrate for about 4 minutes. To prevent the channel network layer from falling into the chloroform during exposure it was attached to a Mylar adhesive film whose liner has been removed in specific areas such that only the four corners of the channel network layer are in contact with the adhesive (Fig. 21C). The channel network layer was then placed on the standoffs and was

exposed to the chloroform vapor for 4 minutes. After treatment, the channel network layer was removed from the container and peeled away from the adhesive. Fig. 22 illustrates the effect of the chloroform vapor. It removed the bulge around the rim of the channels, smoothened the channel surface profile, and increased optical clarity of the channels.

A

B

C

D

36

E

F
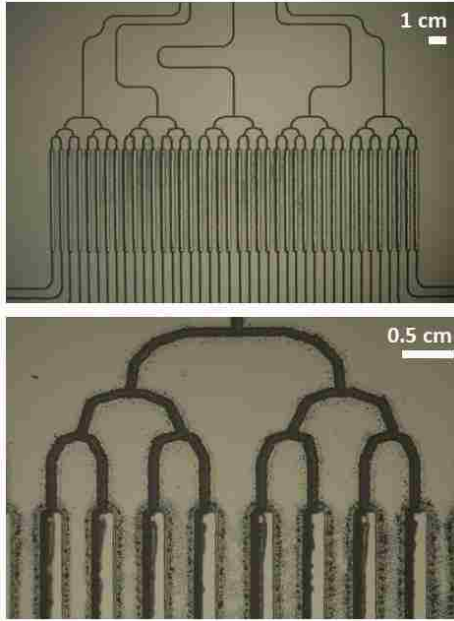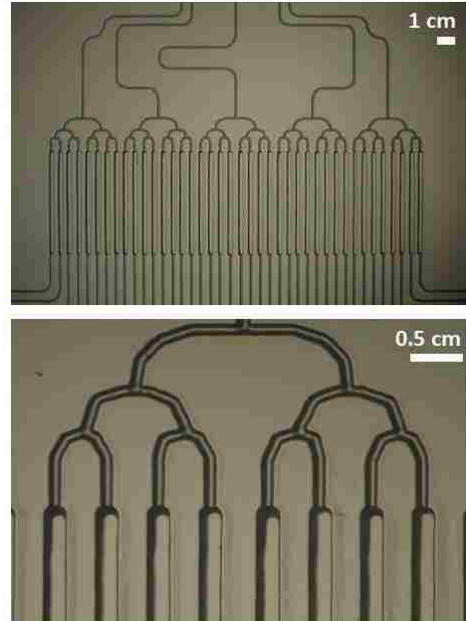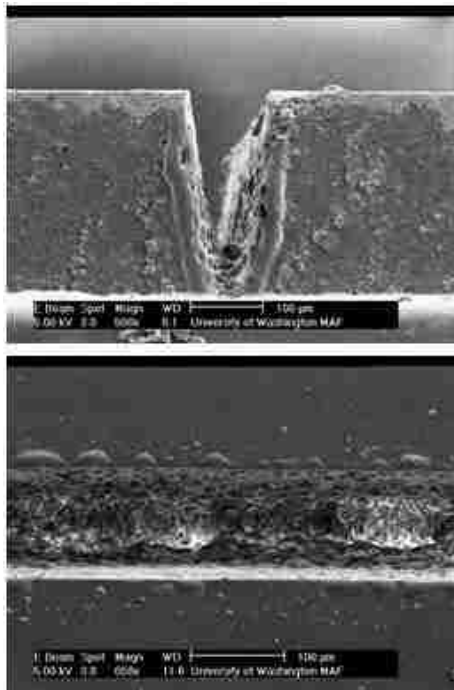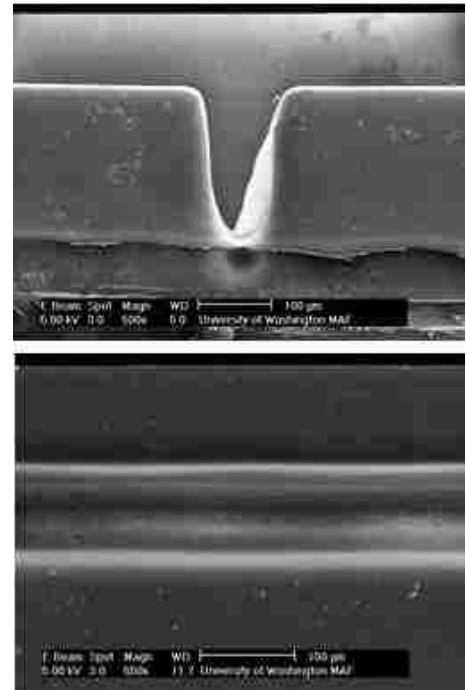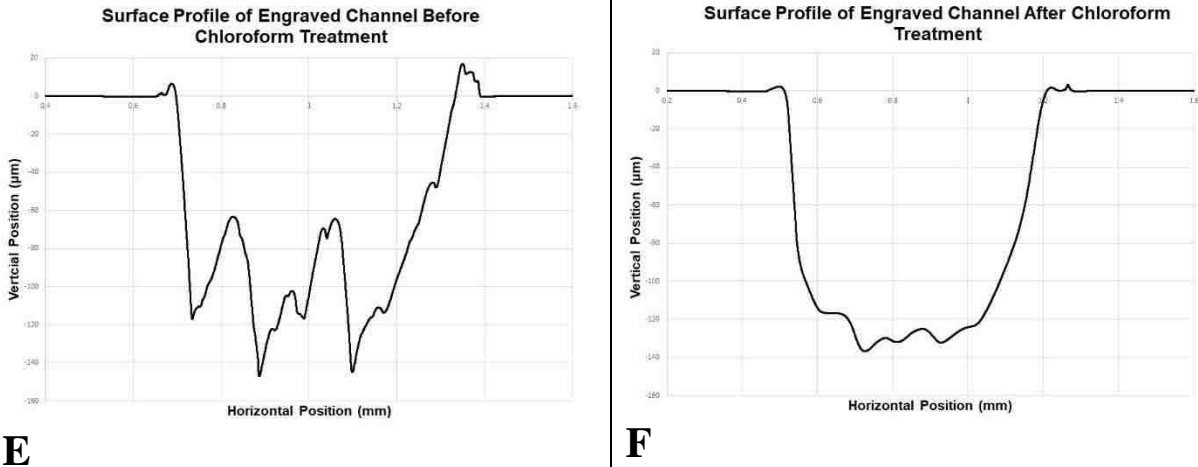
Figure 22: Chloroform treatment of channel network layers. (A) Micrographs of a channel network layer before treatment. (B) Micrographs of a channel network layer after treatment. (C) Cross-sectional and top view scanning electron micrographs of the channel network layer before chloroform treatment. (D) Cross-sectional and top view scanning electron micrographs of the channel network layer after chloroform treatment. (E) Sample profile of channel before chloroform treatment. (F) Sample profile of channel after chloroform treatment.

4.5 Bonding Methods

4.5.1 Conventional Oxygen Plasma Treatment

When the OncoSlice device was primarily made of PDMS, the PDMS layers were bonded together using oxygen plasma treatments. Oxygen plasma serves to expose PDMS to hydroxyl groups which bond to the silicon atoms and make it reactive (Fig. 23). Pressing PDMS against other silicon substrates such as another PDMS layer or glass would cause the formation of strong covalent bonds. Exposure of PDMS to hydroxyl groups also renders the PDMS hydrophilic which is important for wetting of channels. The PDMS version of OncoSlice had four PDMS layers that all had to be exposed to oxygen plasma and carefully aligned and bonded using expensive instruments. This process was not amenable for high throughput manufacturing since the process of aligning and bonding requires very skilled personnel with high expertise in microfluidic device fabrication. A single mistake would render the device unusable and the user would have to start the fabrication process from the beginning.
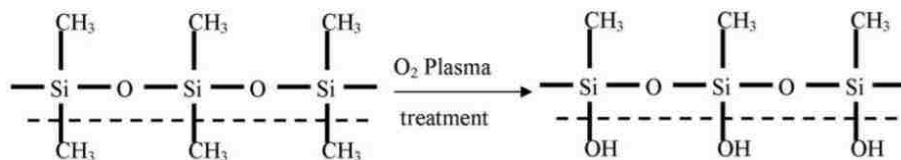
Figure 23: Surface modification of PDMS by oxygen plasma treatment – image reproduced from Ref. 28 with permission from Bentham Science Publisher Ltd.

4.5.2 APTES Treatment

In the previous PDMS-based device, the PDMS through-hole layer had to be bonded to the modified PS 96-well plate. The bonding was done through surface modification of the well plate using a silane solution called (3-aminopropyl)triethoxysilane (APTES). The process for bonding PDMS to a plastic substrate such as PS or PMMA is shown in Fig. 24. Silicon containing bonds

37

were introduced to the well plate by immersing it in an APTES solution that was heated at 80°C and then exposing both the PDMS layers and the well plate to oxygen plasma to obtain silanol groups[29]. The plate and the PDMS were then bonded together by manually pressing them together or by placing a weight over them. This method can theoretically be used to bond two PMMA substrates together if they have both been treated with APTES, exposed to oxygen plasma, and pressed together. However, this method may not be as reliable since the substrates are stiff and hard. They must make good conformal contact to bond well otherwise leaks are a possibility. Simpler methods for bonding the channel network layer to the well plate are further explored in subsequent sections.

PMMA (plexiglass)   PDMS, thermally cured
(a) Surfaces to be bonded

NH₂   NH₂   NH₂

(b) PMMA surface functionalised by APTES

O₂ plasma and
exposure to air

(c) Creation of silanol groups on both surfaces

PDMS

PMMA

(d) Bonded substrates
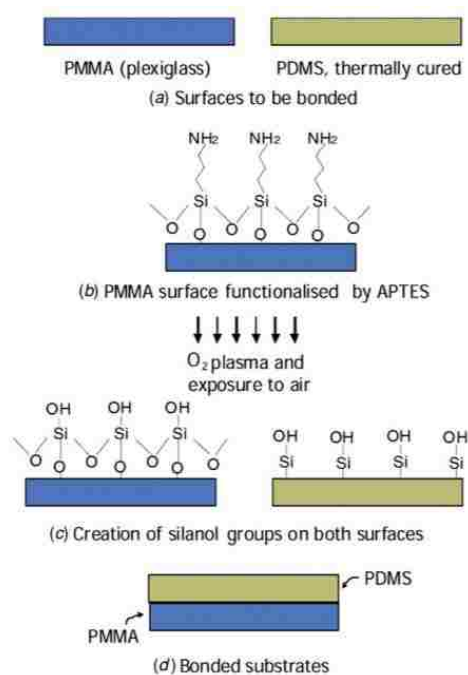
Figure 24: Process flow for bonding PDMS and PMMA substrates using APTES – image reproduced from Ref. 29 with permission from The Institute of Physics Publishing

4.5.3 Adhesives for the Assembly of Microfluidic Layers

4.5.3.1 PSA Films

Pressure-sensitive adhesive (PSA) films are one alternative to surface modification techniques for bonding. These films have a polymer layer that can flow at room temperature which wets the surfaces to be bonded thereby creating a strong bond[30]. PSA films are simple to use since they only need to be applied by manual pressure to surfaces to be bonded. No special equipment or chemicals are needed.

Two varieties of PSA films were tested as an alternative to using APTES to bond a laser engraved, PMMA channel network layer to a modified PS 96-well plate. They were an adhesive with silicone adhesive on one side and acrylic adhesive on the other and an adhesive with silicone adhesive on both sides (Adhesive Applications, SA-1020 and SA-1060). The bonding of the PMMA channel network layer to the PS 96-well plate was difficult since both substrates are stiff and do not

conform well to each other when bonded directly to each other with either double-sided adhesive. A PDMS intermediate layer with through-holes to connect the wells to the channel network layer was used to provide a more compliant surface to which the plate and channel network layer could adhere (Fig. 25). The PSA films were tested to see which could bond the PDMS best to the well plate and the PDMS to the PMMA channel network layer. Additionally, since the OncoSlice device was placed in a cell culture incubator during most of its operation. The wells of devices assembled with these PSA films were filled with phosphate buffered saline (PBS), a common solution used in cell and tissue culture, and the devices were placed in a cell culture incubator set to 37˚C for 12 or more hours to see if the bond remained strong. The PSA films adhesives were cut out using the VLS 3.60 laser cutting system, and they were adhered to the PDMS through-hole layer manually. The best PSA film for bonding the well plate to the PDMS was the one with silicone adhesive on both sides and the best PSA film for bonding the PDMS to the channel network layer was the one with silicone adhesive on one side and acrylic adhesive on the other (Fig. 25). This bonding method caused no leaks but the need for the molding and curing of PDMS and punching out of holes remained a cumbersome, tedious step. Bonding techniques that precluded the need for PDMS layers were explored further.
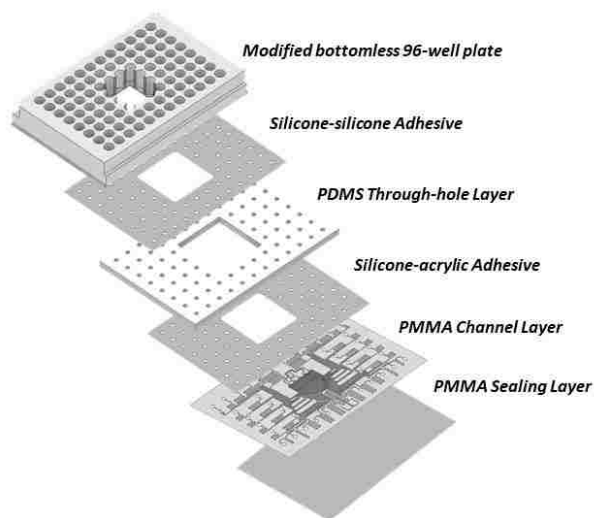
Figure 25: Bonding of device layers using double-sided adhesives

4.5.3.2 300 LSE

During the transition to an all-PMMA platform, the PS 96-well plate was transitioned to a PMMA well plate that could hold more volume in each well. A well plate that can hold more volume was more convenient because it increased time in between refills. The first version of the PMMA plate was composed of three 6.35 mm thick PMMA layers. To bond these layers together, an adhesive called 300 LSE (low surface energy) by 3M technologies was used. This adhesive is used to bond low surface energy plastics such as PMMA together. An adhesive must be able to spread over a substrate's surface to adhere to it strongly. This is called "wetting out." The ability of an adhesive to wet out over a surface depends on the surface energy of the solid. If the surface energy of the substrate is higher than the surface energy of the adhesive, then the adhesive will wet out over the

surface and bond strongly to the substrate. The opposite happens if the surface energy of the substrate is lower. PMMA is a low surface energy plastic that makes it difficult to bond to other plastics, but 300 LSE can overcome this. Plates were cut out from a 6.35 mm thick PMMA sheet. Prior to cutting plates, a sheet of double-sided 300 LSE was adhered to one side of the PMMA sheet and cut along with the plates. When they were cut out, the plates already had a side that could be adhered to another PMMA piece and the 300 LSE did not need to be aligned and manually applied. The three PMMA layers were bonded together with the 300 LSE and were pressed together by hand to form the well plate. The well plate was then also adhered to the channel network layer using the same adhesive (Fig. 26A). The 300 LSE prevented leaks between wells and was not affected by the conditions of the cell culture incubator. However, during use of the device on tissue samples, some channels became occluded and prevented solution from flowing into their corresponding lanes. This changed the overall hydraulic resistance of the channels and the flow rates within each individual channel, making some flow faster than others. The occlusion came from small pieces of the 300 LSE adhesive that came loose during laser cutting (Fig. 26B). This phenomenon often happened with devices assembled with 300 LSE, so bonding methods that do not utilize adhesives such as chemical bonding were explored.

A **B**
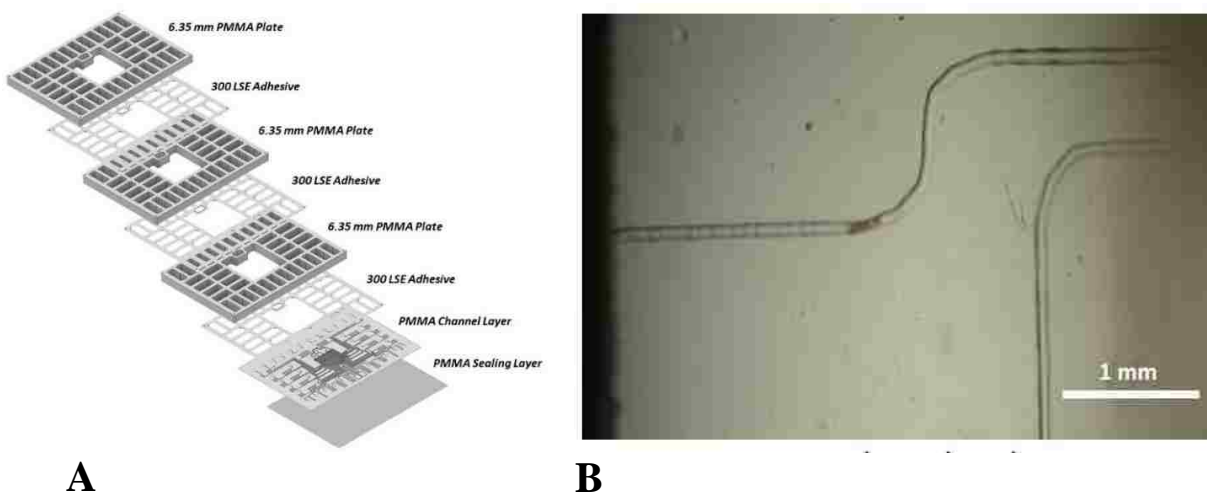
Figure 26: Bonding of device layers using 3M 300 LSE adhesive. (A) Layer-by-layer schematic of OncoSlice device assembled with 300 LSE adhesive. (B) Debris from laser cutting 300 LSE adhesive occluding a channel.

4.5.4 Lamination Techniques

4.5.4.1 PMMA/PET

Lamination techniques have previously been used to develop simple microfluidic devices made of plastic. This technique usually entails the use of laser cutting features/microchannels onto a PET film and sealing them using blank sheets of PET and an office laminator. The laminator serves to heat the PET close to its melting point causing the polymer bonds break and it presses layers of the PET together such that when they exit the laminator and begin to cool, the layers bond together[31]. This approach was applied to fabricate the channel network layer.

The channel network layer was fabricated by engraving channels onto PMMA substrates with the VLS 3.60 laser cutter. This layer and a sheet of PET were then fed into an office laminator (Akiles

ProLam Ultra X6). Multiple combinations of temperature and roll speed settings were tested to see which provided a strong bond while also keeping the channels open. Optimal temperature and speed settings were found that kept the channels open, however, the bond between the PET and PMMA was weak. The channel network layers produced were tested for their durability when immersed in PBS for 12 hours in a cell culture incubator set to 37°C (Fig. 27A). None proved to be durable as the PET floor could be easily peeled away from the PMMA channel network layer (Fig. 27B). The weak bond was attributed to the PET and PMMA being too dissimilar to be bonded together.

4.5.4.2 PMMA/PMMA

After the lamination of the PMMA channel network layer with a PET floor proved to be ineffective, lamination of a PMMA floor was attempted instead of a PET floor. Multiple combinations of temperature and roll speed settings were again tested. Though optimal temperature and speed settings were found, and the channel network layers produced were durable while immersed in PBS in a cell culture incubator, upon closer inspection of the channels, some of the channels had irregular curves when they should be straight lines (Fig. 27C). It was also observed that tiny air pockets formed during lamination indicating that the PMMA did not bond in those areas and so liquid entering that area spread across the air pocket. Due to these results, it was concluded that lamination techniques were not appropriate for the fabrication of the OncoSlice device.
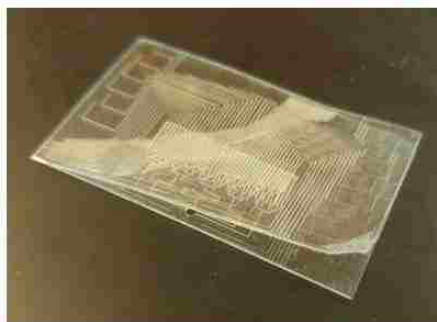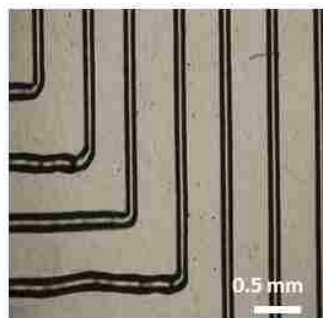
Figure 27: Sealing channel network layers using lamination. (A) Process flow for testing efficacy of lamination technique. (B) Peeling of PET laminate from PMMA substrate after lamination and immersion on PBS. (C) Channel irregularities after lamination of PMMA substrate with PMMA laminate.

4.5.5 Solvent Bonding

4.5.5.1 Sealing the Channel Network Layer Using Chloroform

The use of PSA films to bond plastic substrates was an indirect bonding method. Direct bonding methods include thermal fusion bonding, solvent bonding, and surface treatment modifications. Solvent bonding techniques are currently used to both seal the channel network layer and bond the channel network layer to the well plate and are discussed in this section.

An appropriate solvent for PMMA was chosen by comparing the Hildebrandt solubility parameters of potential solvents with that of PMMA. The Hildebrandt parameter is a measure of the cohesive molecular forces within a material[30]. If the Hildebrandt parameter of a solvent and solute are similar, then their respective cohesive forces are similar, and they will tend to not separate from one another. The Hildebrandt parameter of PMMA and a few relevant solvents are shown in Table 6. Ethanol and IPA have previously been used by Bamshad et al. to seal laser micromachined channels in PMMA[34]. However, this study had to heat the ethanol and IPA to reduce their solubility parameters to match that of PMMA since their parameters at room temperature are higher than that of PMMA. This adds another processing step that is not ideal. Additionally, use of a solvent in its liquid phase can be difficult to control because it may cause channel deformation. Chloroform has previously been used in other studies to bond PMMA substrates together for microfluidics[33]. Its solubility parameter is the same as PMMA, so it is a strong solvent for PMMA. As such, immersion of PMMA with engraved channels into chloroform will cause channel deformation. A more appropriate technique would be to immerse a blank piece of PMMA in chloroform and then let it dry. Then PMMA with engraved channels can be mated with the blank piece and then thermally pressed together for bonding. Another technique would be to expose PMMA to chloroform vapor and then thermally press it to a blank substrate. The latter technique was used in this study.

Table 6: Solubility Parameters of PMMA and Relevant Solvents[32]

Material	Hildebrandt Parameter (MPa$^{1/2}$)
PMMA	19.0
Chloroform/Trichloromethane	19.0
Methylene Chloride/Dichloromethane	19.8
Ethanol	26.0
IPA	23.8

Our method was adapted from Ogilvie et al. and the setup and process for chloroform exposure was explained in Section 4.4.2[20]. Chloroform has been shown to reduce surface roughness in PMMA microchannels due to polymer reflow. When the polymer is in a reflow state, the surface of the PMMA is soft such that when it comes into contact with another PMMA substrate that has

also been exposed to chloroform, the polymers within the two substrates will bond to each other as the vapor evaporates from their respective surfaces.

The laser engraved channel network layer was exposed to chloroform vapor for 4 minutes. After, a 125 μm PMMA film (i.e. the sealing layer) with the same dimension as the channel network layer was exposed to chloroform vapor for 2 minutes. The film was then carefully hand pressed onto the channel network layer which forms a weak bond. The two layers were then sandwiched between two 3.18 mm thick PDMS slabs with the same outer dimensions as the channel network layer. The whole assembly was then placed in a heat press preheated to 60°C and pressed for 10 minutes between 120-160 psi (Fig. 28). The platens do not conform well to the PMMA due its stiffness, so the PDMS slabs serve to distribute pressure more evenly across the channel network layer and the sealing layer while being pressed. The PDMS slabs can be reused to press several more channel network layers.
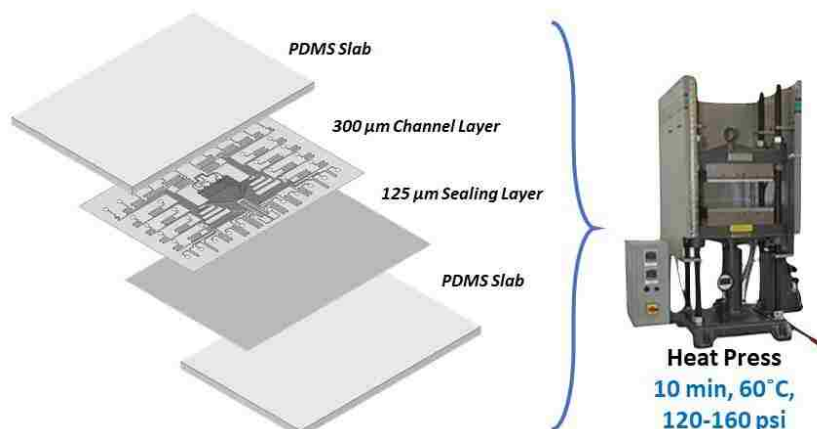
Figure 28: Sealing of the channel network layer using chloroform solvent bonding within a hydraulic heat press

For any solvent bonding process, variable parameters must be optimized for each specific application since there are different grades of PMMA and they may react differently to different solvents. To seal the channel network layer using chloroform solvent bonding, pressure, temperature, exposure time of the sealing layer to chloroform, and time of pressing with heat were varied to find the optimal parameters that yielded open and sealed channels. The process undertaken to find these parameters is described in Table 7.

Table 7: Optimization of Parameters to Seal Channel Network Layer

Pressure (psi)	Temperature (°C)	Sealing Layer Chloroform Exposure Time (min)	Pressing Time	Sandwiched with PDMS?	Results (Percent of channels occluded)
200-240	65	3	1 min with heat, 10 min cool down	No	~50%

43

Pressure (psi)	Temperature (˚C)	Sealing Layer Chloroform Exposure Time (min)	Pressing Time	Sandwiched with PDMS?	Results (Percent of channels occluded)
160-200	65	3	1 min with heat, 10 min cool down	No	~50%
120-160	65	3	1 min with heat, 10 min cool down	No	~2.5-25%
120-160	60	2	1 min with heat, 10 min cool down	Yes	0%
120-160	60	2	10 min with heat	Yes	0%

4.5.5.2 Bonding the Channel Network Layer and the Well Plate Using Methylene Chloride

Bonding of the 40-well plate to the channel network layer was very simple. The 40-well plate was prepared by exposing the bottom side of the plate to chloroform vapor for 30 minutes using the chloroform setup described in Section 4.4.2. This reduced any surface roughness caused by laser cutting. The vapors were then left to evaporate off the plate for 10 minutes. A glass container was then filled with 20 mL of a commercial liquid acrylic adhesive called Weld-on 4 by Scigrip. This adhesive is mostly composed of a solvent called methylene chloride. Methylene chloride is an appropriate solvent because its solubility is similar to that of PMMA (Table 6). Weld-on 4 was chosen because it has other agents that accelerate the bonding process, so plates can be fully bonded to channel network layers within minutes. The solvent softens the surfaces of substrates to be bonded, and as it evaporates it bonds the substrates together. The plate was dipped in the Weld-on 4 solution for 15 seconds. Nitrogen was blown in the outlet tubing hole to remove excess solvent and prevent it from dissolving the outlet in the channel network layer. The channel network layer was then aligned such that its outlet hole was within the outlet hole of the plate. The outlet hole of the plate has a larger diameter than the outlet hole of the channel network layer, so alignment was done easily by eye. The channel network layer was hand pressed onto the plate. A 500 μm thick blank PMMA sheet with the same outer dimensions as the channel network layer was placed on top of the channel network layer and the whole assembly was sandwiched between two PDMS slabs. The whole assembly was then placed in a hydraulic press (Fig. 29) and pressed at 200 psi for 5 minutes. The 500 μm blank PMMA sheet served to provide some rigidity to the assembly as it was being pressed. Without it, the PDMS slab would press into the flexible channel network layer and crack it. After assembling and pressing, outlet tubing was ready to be added to the device.
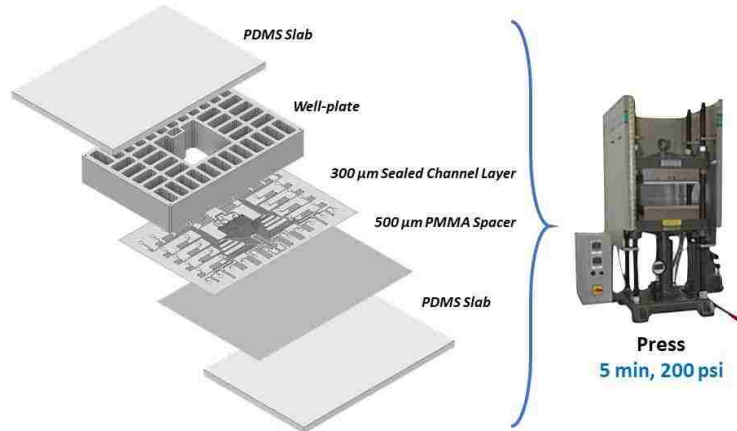
Figure 29: Assembly of the OncoSlice device in a hydraulic press

4.6 Outlet Design

4.6.1 PDMS Molded Outlets

The previous PDMS-based version of OncoSlice also had an outlet composed of PDMS. A molded block of PDMS was bonded to the microfluidic chip layer with double-sided adhesive and a hollow metal needle pin was inserted into the PDMS. The metal needle connected the outlet of the microfluidic chip layer to external tubing that was connected to a syringe pump that facilitates fluid flow in the device. This approach, however, was not sturdy as the outlet could easily be removed if the pin was accidentally pushed over (Fig. 30A). Removal of the metal pin was the logical next step, and molding tubing within PDMS as it cures was our next approach.

A fixture to mold PDMS with tubing inside was created by laser cutting several plastic layers: a mold roof, the main mold, and a mold floor (Fig. 30B). Tubing was threaded through the mold roof and the main mold and was secured in place to the mold floor. The mold floor had protrusions that were inserted into the tubing and held them in place. The main mold was filled with PDMS pre-polymer and the mold roof clamped on top. The fixture was then placed in a 65˚C oven for about 2 hrs. Then the mold roof and the main mold were carefully removed, and each outlet was removed from the mold floor. Double-sided silicone-acrylic tape with a hole the same diameter as the outer diameter of the tubing was cut out and was placed on the bottom of the outlet to attach the outlet to the device.
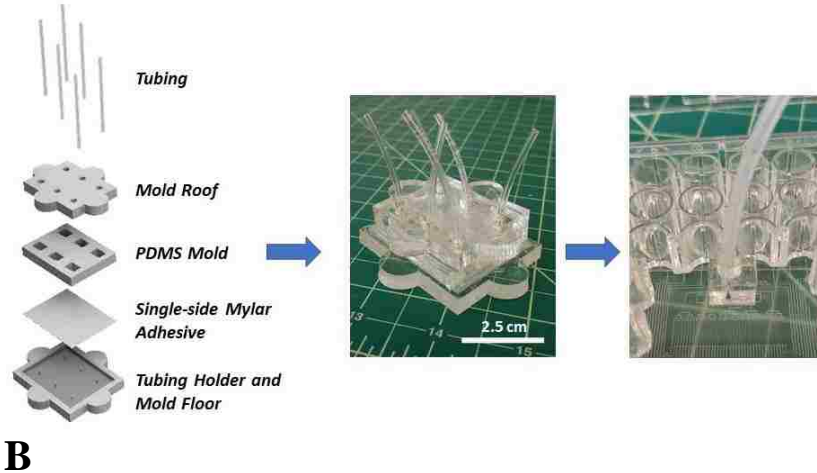
A

45

B

The mold roof was cut from PMMA and has six holes in it through which tubing was threaded and it served to keep the PDMS flat as it cures. The main PDMS mold was also cut from PMMA and has six rectangular shapes cut through it so that the cured PDMS had a cuboid shape. The mold floor was also cut from PMMA and had an area that had been raster cut to leave six protrusions that were inserted into the tubing to hold it in place as the PDMS cures. Raster cutting the mold floor did not leave a smooth surface, so PDMS molded to this surface was also not smooth. To alleviate this, a piece of single-sided mylar adhesive with six holes that match the protrusions in the mold floor was placed over the mold floor.

Though this approach of incorporating tubing into the PDMS outlet has advantages over the previous design, the preparation and curing of PDMS greatly increases the overall fabrication time per device. Additionally, applying double-sided tape to the bottom of the outlet was not a robust method of securing the outlet to the device as the outlet can still be easily removed.

4.6.2 Outlets Integrated into the PMMA Well Plate

With the transition from using a PS 96-well plate to a PMMA 40-well plate, our next approach was to incorporate the outlet directly into the well plate. Transitioning from the use of a standard PS 96-well plate to a PMMA plate allowed for design changes to be made that were realized through changes in a CAD file. An outlet could be integrated into a three-layer plate or a single-layer plate. In a three-layer plate, the bottom plate had a hole cut out that matched the outer diameter of the tubing. The top two plates had a rectangle cut out that had a much larger area than the hole in the bottom plate. When the top two plates were assembled together, they formed a well around the outlet hole in the bottom plate. After inserting tubing into this hole, the well was filled with a sealant to secure the tubing in place and provide an air-tight seal (Fig. 31A). In a single-layer plate, a well was rastered on the top of the plate (Fig. 31B). There was a hole in the well that matched the diameter of the outlet tubing and went down from the bottom of the well to the bottom of the plate. Tubing was placed into this hole and the well was filled up with sealant to secure it.
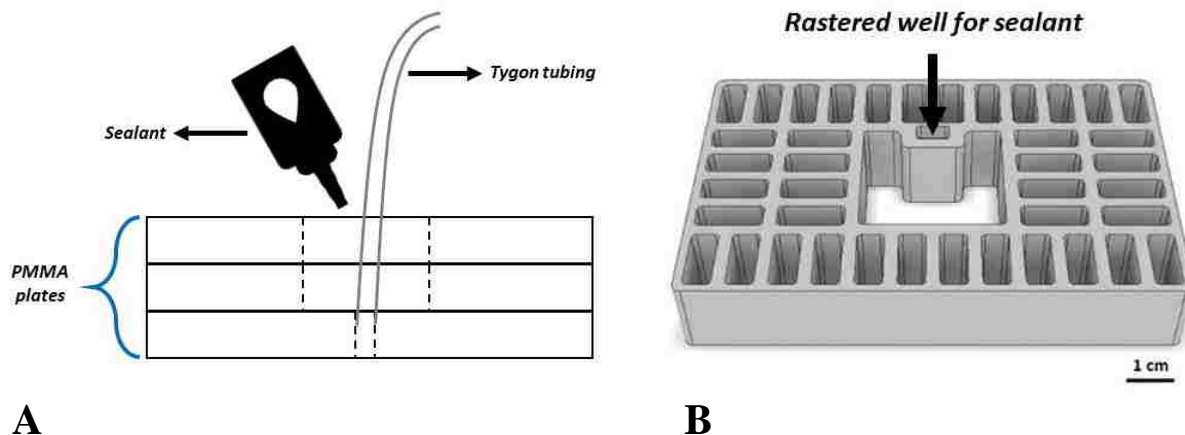
A **B**

We have tried several sealants to see which provided the most stability to the tubing and an air-tight seal: Gorilla super glue, Duco cement glue, and a silicone marine sealant. All three provided an air-tight seal. This was tested by immersing the bottom of the outlet in water and applying negative pressure to the tubing using a vacuum line. If the seal was not air-tight, then the vacuum pulled in the surrounding air which caused a hissing noise and air bubbles could be seen in the vacuum line. Gorilla super glue provided the strongest seal since the tubing was not able to be removed from the outlet by manual force, which was not the case for the other two sealants. After insertion of the tubing and the addition of the lid and base, the device is ready for use with tissue samples.

4.7 Device Characterization

4.7.1 Fluorescent Dye Delivery

To illustrate that dugs could be spatially delivered to intact tissue through the open drug lanes with limited cross-talk, three fluorescent nuclear staining agents were added to specific wells and a syringe pump was used to pull them towards the open drug lanes. Atop the lanes sat an intact U87 tumor slice (Fig. 32A). Dyes of different colors were used: Hoechst (blue), CellTracker Green CMFDA, and CellTracker Red CMPTX. Each staining agent was separated by a buffer lane containing PBS and the slice was exposed for one hour at a flow rate of 2 mL/hour. The dyes remained separated and exhibited little lateral diffusion (Fig. 32B). Side view fluorescence images were taken to demonstrate penetration depth of the agents into the tissue (Fig. 32C and D). Within one hour the dyes were already diffusing upward. Prolonged exposure would increase this trend.
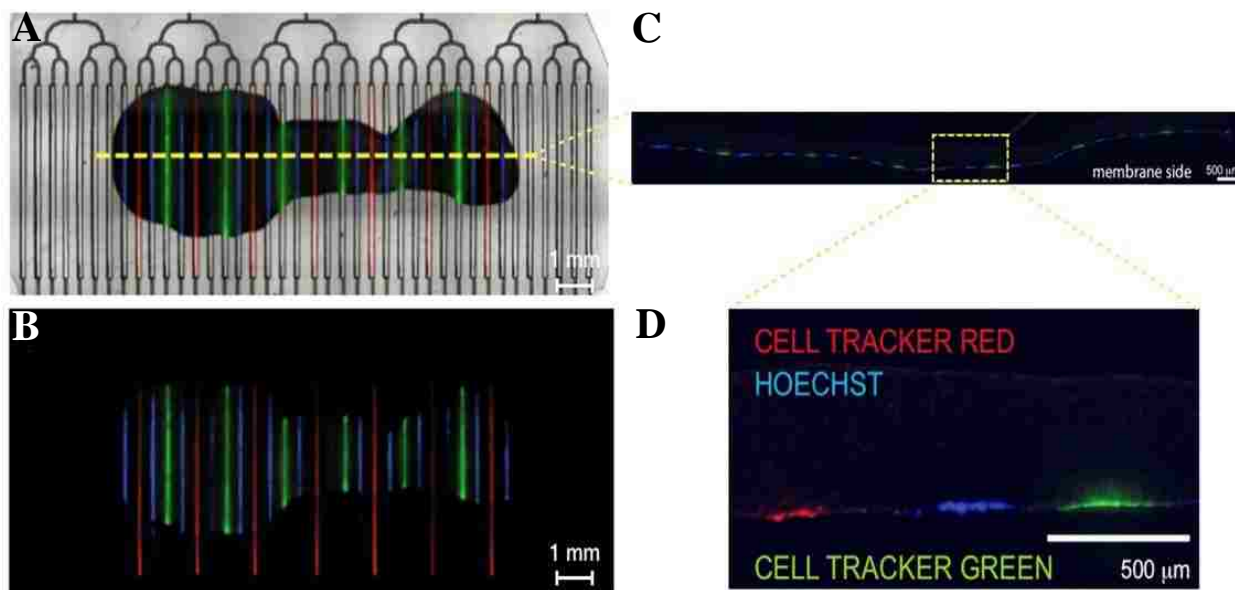
Figure 32: Fluorescent dye delivery. (A) Brightfield and fluorescence image showing spatial delivery of nuclear staining agents through open drug lanes to U87 tumor slice. (B) Fluorescence image showing limited cross-talk between staining agents. (C) Fluorescence image of side view of tumor slice. (D) Magnified view of side view of tumor slice showing vertical diffusion of staining agents.

4.7.2 Device Performance Characterization

In order to understand how well our fabrication protocol is able to produce both similar channels within a single device and similar channels across multiple devices, we took several devices and filled their wells with alternating red and blue food coloring dyes. The devices were then connected to a syringe pump and run at different flow rates (Fig. 33). To determine variability in hydraulic resistance for each channel, the individual flow rates for each channel were calculated and compared.

Figure 33: Performance testing setup

48

In one testing run, three devices were tested. Each well was filled with 1 mL of dye. They were all run at a flow rate of 10 mL/hour for one hour and then subsequently the flow rate was changed to 2 ml/hour, and the devices were run for three more hours. After, the volume left in each well was measured and used to calculate overall flow rate within each channel for each device. The percent standard deviation of the flow rates for each device was calculated and indicated the variability of the flow rates within a single device. Comparison of percent standard deviations can be used to compare the variability of devices to one another.

Table 8: Intra- and Inter-Device Variability Comparison

	Device 1	Device 2	Device 3
Syringe Setting	10 ml/hr (1 hour) → 2 ml/hr (3 hours)		
Standard deviation (%)	4.21	8.04	6.71

For the three devices tested in Table 8, Device 1 had the lowest percent standard deviation in flow rates in its channels indicating that the channels in this device were very similar to one another. For Devices 2 and 3, their percent standard deviations were higher indicating that the channels within each respective device were more variable than the channels in Device 1. However, the percent standard deviations were more similar for Devices 2 and 3 indicating that these devices performed similar to one another than when comparing each respective device to Device 1. Repeating this performance test for more devices remains to be completed.

Table 9: Comparison Between High and Low Flow Rates Within a Single Device

	Device 1	
Syringe Setting	10 ml/hr (2 hours)	1 ml/hr (16 hours)
Average Flow Rate (µL/hr)	266.54	27.05
Standard deviation (%)	11.31	10.6

To determine whether high and low flow rates set on the syringe pump induced more variability in flow rates, a single device was run two separate times each at different flow rates. In the first testing run, each well in the device was filled with 1 mL with alternating red and blue food dyes and run at 10 mL/hour for 2 hours. The device was then stopped, and the volume left in each well was measured and used to calculate flow rates for each well. This procedure was then repeated at for a flow rate of 1 mL/hour for 16 hours. The results in Table 9 show that the percent standard deviations for each flow rate are very similar which indicates that a difference between high and

low flow rates does not induce more variability. This is only for one device however. Comparison across multiple devices for high and low flow rates remains to be completed.

4.7.3 Lateral Diffusion Assessment Within the PTFE Membrane

Lateral diffusion of drugs in the membrane must be limited to prevent cross-talk and is related to the flow rate set on the syringe pump. A low flow rate would allow the device to be run for longer before the wells need to be refilled. A low flow rate, however, also causes more lateral diffusion of drugs in the PTFE membrane. Cross-talk of drugs in the membrane is not ideal since this prevents discrete spatial delivery to tissue samples and prevents assessment of the effects of individual drugs.

A minimum flow rate that prevents lateral diffusion was determined by flowing a fluorescent solution called fluorescein (100 mM) into channels/lanes with numbers 4, 11, 18, 25, 31, and 38. These lanes were chosen to assess the diffusion of fluorescein into the blank lanes one, two, and three lanes away on either side of the fluorescein-containing lanes. The blank lanes only contained PBS. When the device is filled with drugs, the drugs are spaced two lanes apart, with the blank lane in between acting as a buffer. A minimum flow rate was determined by assessing the fluorescence intensity two lanes away on both sides of the fluorescein-containing lane at different flow rates. In an experiment, these lanes would contain another drug, so a flow rate should be chosen that limits fluorescence in these lanes. Flow rates of 10, 1, 0.75, 0.4, 0.3, 0.2 and 0.1 ml/hour were tested. The syringe was left to equilibrate for 5 to 10 minutes after changing the flow rate of the syringe pump before fluorescence images were taken. For each flow rate, images were taken of each lane containing fluorescein at unsaturated (7 ms) and saturated (70 ms) exposure times. The 70 ms exposure time allows for increased sensitivity of the lanes on either side of the fluorescein-contain lanes. For each image, three different regions of the lanes were analyzed: downstream of the flow, middle of each lane, and upstream of the flow (Fig. 34). Fluorescence intensity profiles were taken for each region.
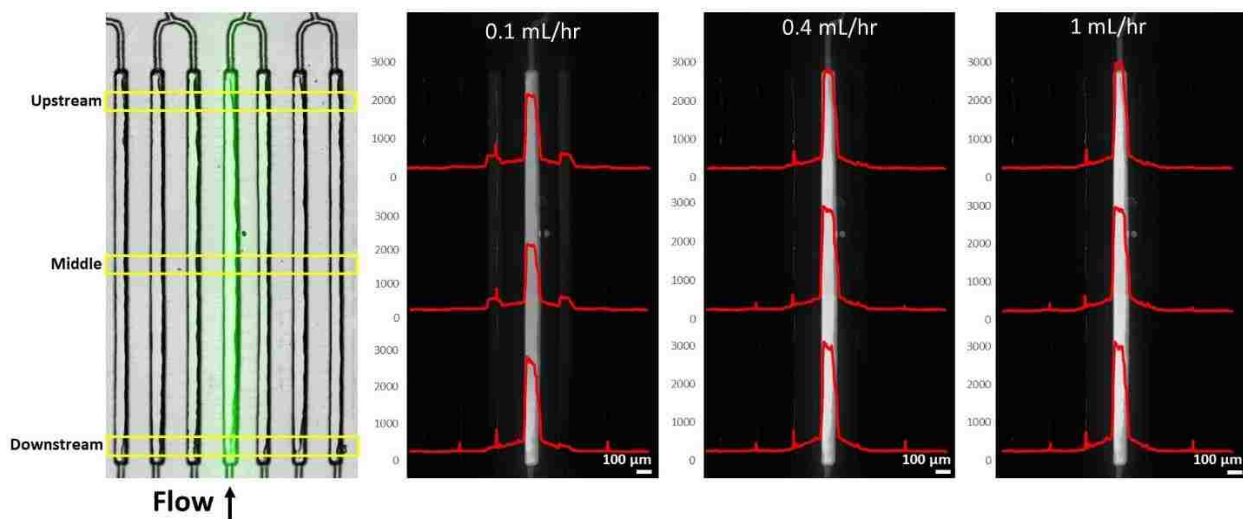
Figure 34: Fluorescence images to assess lateral diffusion in the PTFE membrane at different flow rates and within different regions of the drug lanes. Fluorescence intensity profiles were taken for each region and for each flow rate tested.

In all the images taken for each fluorescein-containing lane at each flow rate, values of fluorescence intensity were measured in each of the three regions of interest (upstream, middle, and downstream) not only in the fluorescein-containing lane but also in the blank neighboring lanes one to three lanes over on either side. These values were corrected to remove background fluorescence. To match the 7 ms data with the 70 ms data, the 7 ms data was adjusted by a correction factor. For each flow rate, the values for each region of interest were averaged for the fluorescein-containing lanes and the lanes spaced one to three lanes away. The 7 ms data and the 70 ms data were then pooled together. The averages of fluorescence intensity in each region of interest for the fluorescein-containing lanes were taken from the 7 ms data, while the averages fluorescence intensity in each region of interest for the lanes spaced one to three lanes away were taken from the 70 ms data. These averages were then normalized to the average fluorescence intensity of the fluorescein-containing channels. Fig. 35 illustrates the results of the image analysis.
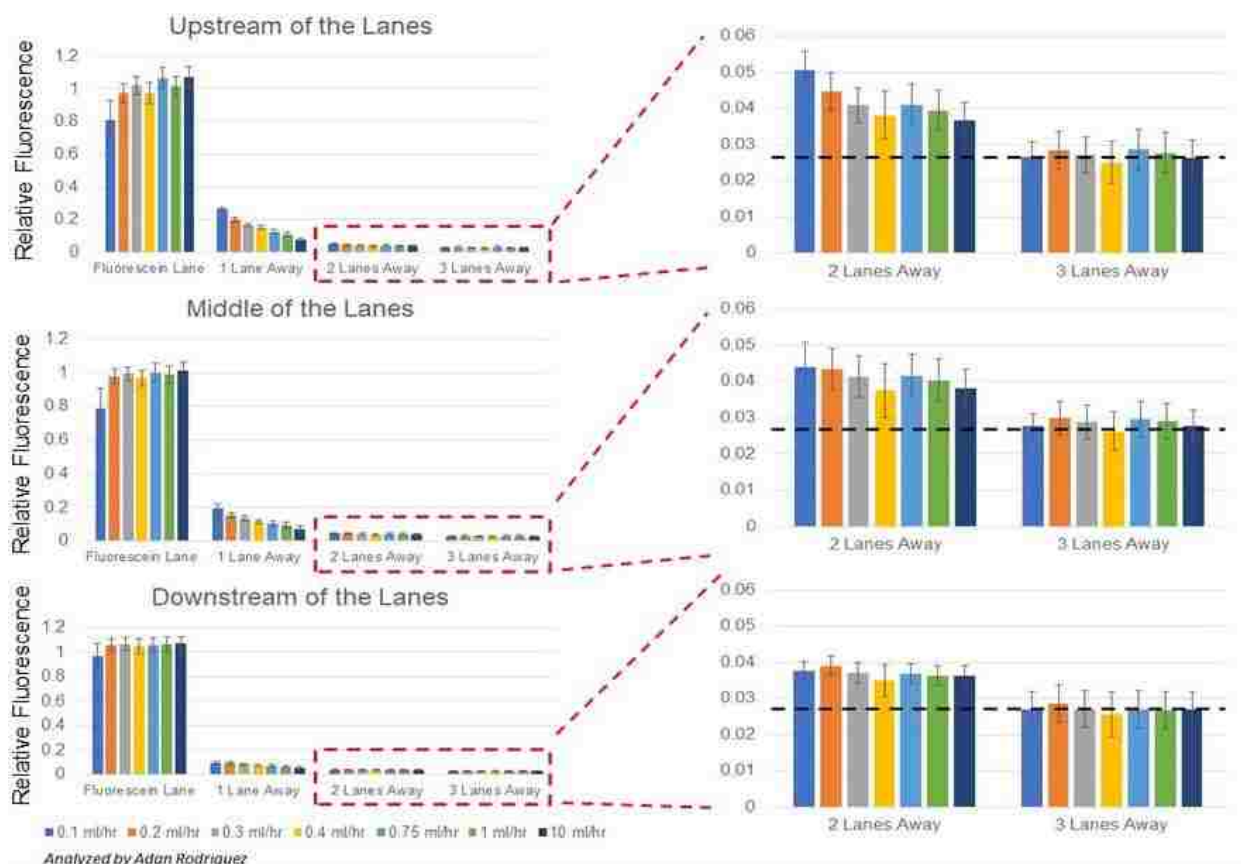
Figure 35: Analysis of lateral diffusion one, two, and three lanes away from the lanes containing fluorescein

There is significantly less fluorescence intensity the further a blank lane is from a fluorescein-containing lane. There is higher fluorescence for lower flow rates indicating that lower flow rates induce more lateral diffusion. Additionally, for all the lanes, there is more lateral diffusion upstream in a lane than downstream, since there is higher fluorescence upstream. This is because the fluid velocity is faster downstream than upstream.

In Fig. 35, the right column shows magnified graphs of the fluorescence intensity in lanes spaced two and three lanes away from a fluorescein-containing lane. The dashed line indicates the relative zero or baseline fluorescence, which is the smallest signal detected in the downstream region of the lanes spaced three lanes away from the fluorescein-containing lanes at 10 ml/hour. Lanes spaced two away from a fluorescein-containing lane were only about 2% more fluorescent than the relative zero, with a flow rate of 0.1 mL/hour showing the most fluorescence and 10 mL/hour showing the least. This is not a significant difference. Upstream in a lane spaced two away, there is a trend of decreasing fluorescence and therefore decreasing lateral diffusion from low to high flow rates. 10 mL/hour is too fast of a flow rate and would make the OncoSlice device inconvenient to use since the wells would have to be refilled almost every three hours if the wells were each filled with 1 mL of drugs. With 1 mL/hour, the device would have to be refilled about every 32 hours if each well was filled with 1 mL of drugs. This is more convenient for the user and an insignificant amount of cross-talk would occur between drugs.

4.8 Conclusions

Here, we have demonstrated a fabrication protocol for the OncoSlice device based on laser micromachining and solvent bonding of PMMA layers. Our protocol is a highly efficient, cost-effective method for more high-throughput manufacturing since fabrication time has been reduced from four days to about two hours and the materials used are inexpensive. Laser micromachining is much faster and easier than soft lithography and compared to the previous PDMS-based fabrication protocol, our protocol has a reduced number of layers that are easier to bond. The PDMS-based device has four layers of PDMS and a PS 96-well plate that required a highly-skilled technician to assemble, while the current device only has three PMMA layers that has a large amount of tolerance and can be aligned and bonded by eye. In general, the transfer of fabrication expertise from one person to another is less difficult with our protocol than a PDMS-based protocol.

5. Multi-material Stereolithography for Integrating Biosensors in Biomicrofluidics

5.1 Introduction

3D printing has the potential to generate new biosensor designs with applications in tissue engineering, cell biology, and implantable devices. SL is a 3D printing technique that allows for printing objects from liquid resin in a layer-by-layer process with layers that have micron-size thickness[35]. Resins for SL can be tuned to achieve prints with desired characteristics. Of interest for biosensing are resins that entrap or covalently bind active biomolecules once polymerized[36]. Here, we describe the sequential printing of a hydrogel biosensor within an optically-clear, biocompatible microfluidic channel.

Our simple 3D printed microfluidic channel with an integrated hydrogel biosensor is the first step toward more sophisticated 3D printed biosensing devices. We envision the printing of several biosensor resins within one microfluidic device allowing for multiplexed sensing. Advantages of these devices that could substantially reduce the cost of biosensor development include easy design using 3D CAD software, manufacturable by non-specialized personnel, and same-day use. Thus, we believe that biosensors co-printed within microfluidic channels will lead to new and improved biosensors and biosensing techniques.

5.2 Avidin Entrapment Within Hydrogels Printed Within Microchannels

Multi-material SL printing of biosensors within microfluidic channels required the development of two different SL resins: a hydrogel biosensor resin and a resin to build a microfluidic channel. Both use acrylate photopolymerization of poly(ethylene glycol) diacrylate (PEG-DA) and a UV-visible photoinitiator (Irgacure 819, 0.4% w/w). The biosensor resin contains PEG-DA (MW=575), UV photosensitizer (2-isopropylthioxanthone, 0.1% w/w) (ITX), and avidin conjugated with Texas Red dye (1.5 µM) as a model detection protein. The microfluidic channel resin contains PEG-DA (MW=258), and ITX (0.2% w/w).
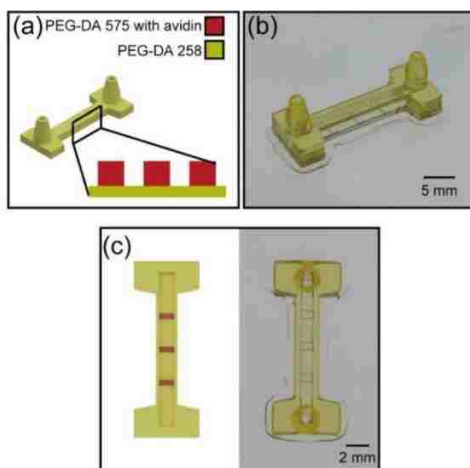
Figure 36: 3D printed microfluidic channel with biosensor strips. (A) CAD representation of microfluidic channel with three strips containing avidin. (B) Photograph of 3D printed channel. (C) Top view CAD representation (left) and top view photograph of 3D printed channel (right).

Using an Ember 3D printer (Autodesk), rectangular biosensor strips were printed within a microfluidic channel (Fig. 36). The setup of the printer and its companion software, Print Studio, are shown in Fig. 37. This printer has an X/Y resolution of 50 μm, Z resolution ranging from 10-100 μm, a build volume of 64 x 40 x 134 mm, and a 405 nm UV light source.

- X/Y Resolution: 50 μm
- Z Resolution: 10-100 μm
- Build Volume (X, Y, Z): 64 x 40 x 134 mm
- 405 nm light source

Figure 37: Ember 3D printer setup

The microchannel was printed on a glass slide (75 mm (L) × 50 mm (W) × 1.0 mm (T)) to make transparent prints. Glass slides were cleaned with acetone, IPA, and deionized (DI) water and dried at 70˚C overnight. The surface of the glass slide was plasma-activated with oxygen plasma for 180 seconds and treated with 3-(trimethoxysilyl) propyl methacrylate (TMSPMA) (Sigma-Aldrich) in an 85˚C chamber for 8 h. The silanized glass slide was attached to the aluminum build plate by coating one side of it with uncured PEG-DA-258 resin and exposing it to UV light using a broadband UV lamp (B-100 A, UVP). The channel and biosensor strips were created in one print and required switching between the two resins (Fig. 38). This process of switching resins has been used in other studies to build porous barriers within 3D printed microfluidic channels[37].
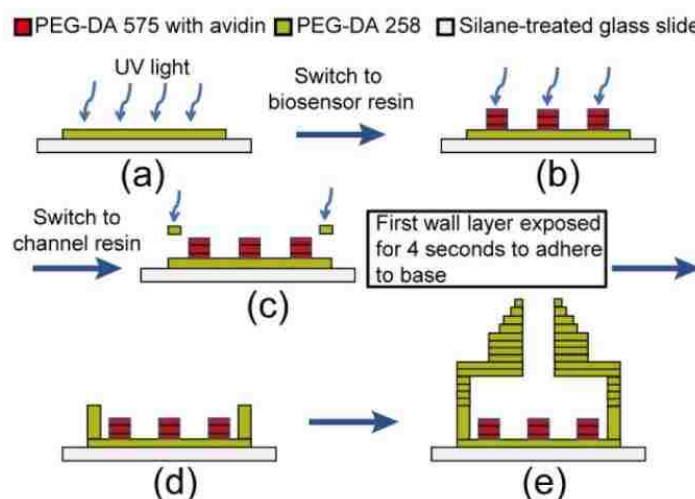
Figure 38: Process flow of printing biosensors within microfluidic channels

All layers in the print were set to be 50 μm thick except the layers of the sensor which were set to be 100 μm thick. Each respective resin tray was filled with enough resin such that the glass slide on the build plate was immersed in the resin while each layer was being polymerized. First, a

channel base was printed. The first layer of the print was exposed for 10 seconds to UV light to create a layer that was strongly adhered to the glass slide and to create a layer that is parallel to the bottom of the resin tray. The glass slide itself may not be parallel to the bottom of the resin tray. In the first layer, the resin between the transparent bottom of the resin tray and the glass slide was polymerized, and this layer conforms to the shape of the bottom of the resin tray and is therefore parallel to it. The next three layers of the base were exposed for 0.8 seconds. Here, the print was paused, and the print was then rinsed with DI water and patted dry. The resin was switched to the biosensor resin. The print was then continued to print the sensor strips. Each 100 μm thick layer of the sensor was exposed for 2 seconds. The print was then rinsed with DI water and PBS, patted dry, and the resin was switched back to the microchannel resin to complete the printing of the channel. At this point in the print, there was a 450 μm gap between the bottom of the resin tray and the channel base, so to polymerize the PEG-DA in between and create the first channel wall layer the exposure setting was set for 4 seconds. Subsequent layers of the channel walls were exposed for 0.8 seconds. All layers of the 200 μm thick channel roof were exposed for 0.3 seconds and all layers of the channel connectors were exposed for 0.4 seconds. The exposure times for each layer are outlined in Table 10.

Table 10: Biosensor Layer-by-layer UV Exposure Settings

Print Feature	Layer Number	Exposure Time (s)
Channel Base	1	10
	2-4	0.8
Biosensor Strip	5-8	2
Channel Walls	9	4
	10-24	0.8
Channel Roof	25-28	0.3
Connectors	29-98	0.4

Fluorescence imaging illustrated that avidin was entrapped after printing the channel (Fig. 39). The image shows that little to no mixing of the two resins occurred since there was little to no fluorescence in the channel walls or connectors. To illustrate that the biosensor resin can detect molecules of interest biotin tagged with fluorescein was flowed into the microchannel and allowed to incubate for 30 min. The avidin has four binding sites for biotin and the complex of the two is the strongest non-covalent interaction between a protein and a ligand. Bovine serum albumin (BSA) at 2% concentration was incubated in the channel prior to the introduction of biotin to prevent non-specific binding. Fluorescence imaging showed that the biotin did not bind to the avidin at all. One possible reason for this was that the polymerized resin was not porous enough to let biotin molecules through to the bulk of the biosensor where the majority of the avidin resides.

Figure 39: Brightfield and fluorescence image of 3D printed biosensor channel with entrapped avidin conjugated with Texas Red dye

5.3 Increasing Porosity of the Hydrogel Biosensor Resin

Other studies have shown the development of porous PEG-DA hydrogels through the incorporation of pore creating agents such as water and non-reactive poly(ethylene glycol) (PEG) of varying molecular weights[38]. Using this concept, several resins were developed that create pores when 3D printed and washed.

A **B**
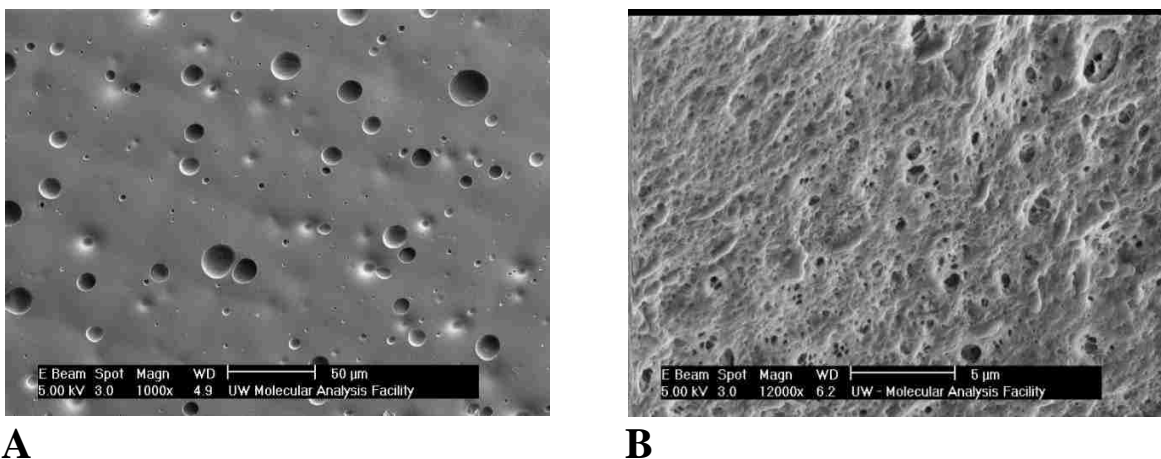
Figure 40: PEG-DA 3D printing resins with increased porosity. (A) Scanning electron top view micrograph of 3D printed strip composed of PEG 8000 in water added to PEG-DA 575 resin at 23% (w/w). (B) Scanning electron micrograph of side wall of 3D printed block composed of PEG 8000 added to PEG-DA 258 resin at 20% (w/w)

PEG (MW=8000) was added to DI water at 30% (w/v). This solution was added at a concentration of 23%(w/w) to a solution of PEG-DA-575 containing Irgacure 819 (0.4% w/w). Strips of this resin were 3D printed onto a glass slide and then soaked in DI water for 24 hours. After, the strips were washed with a graded series of ethanol washes ranging from 40% to 100% in increments of 20% each for 20 minutes in a rocker. The strips were then imaged using a scanning electron microscope. Fig. 40A illustrates that this resin indeed does have pores. The image, however, is the top view of the strips. A more representative depiction of pores would be a cross-sectional image. Another porous resin developed also consisted of adding PEG-8000 to a solution of PEG-DA-258 at a concentration of 20% (w/w) by first diluting it in water at 30% (w/v). A block of this resin was 3D printed and then broken in half to view the porosity along the side wall of the block. This resin produced interconnected pores with diameters less than 5 μm. (Fig. 40B). It should be noted that scanning electron micrographs do not accurately represent the pores of these hydrogels since the samples were dried before imaging which causes the pore dimensions to change due to loss of

56

moisture. When in use, the microchannel would be filled with liquid solutions, and the solutions would cause the hydrogel biosensors to swell and the pore sizes to increase. A better understanding of the pore sizes of a hydrogel would be to study how molecules of different sizes are able to be transported to the bulk of the resin through diffusion. Characterization of the resins developed in this research with this method remains to be performed. Nonetheless, the scanning electron micrographs do show that pores do exist within these resins when polymerized.

5.4 Biotin-binding Assays Using Porous Biosensor Strips Within a Microchannel

Utilizing PEG-8000 as a porogen, a new biosensor resin was developed. It contained PEG-DA (MW=700) which has increased void sizes in its mesh network compared to PEG-DA-575 due to its higher molecular weight. The resin also contained PEG-8000 (20% w/w) and Irgacure 819 (0.6% w/w). This resin is highly porous and would lead to the avidin possibly leaching out instead of being entrapped. Covalently bonding biomolecules into the PEG-DA mesh network would overcome this. As such, this new biosensor resin also contained biotinylated PEG molecules (MW=5000) that have reactive acrylate groups that bind to the mesh network after exposure to UV light. These molecules were added at a concentration of 0.0001% (w/w). The biosensor strips were printed with 50 μm layers with each layer being exposed for two minutes. It takes a longer time to polymerize the mesh network due to there being less acrylate reactive sites. The channel base, walls, and roof were printed as before.
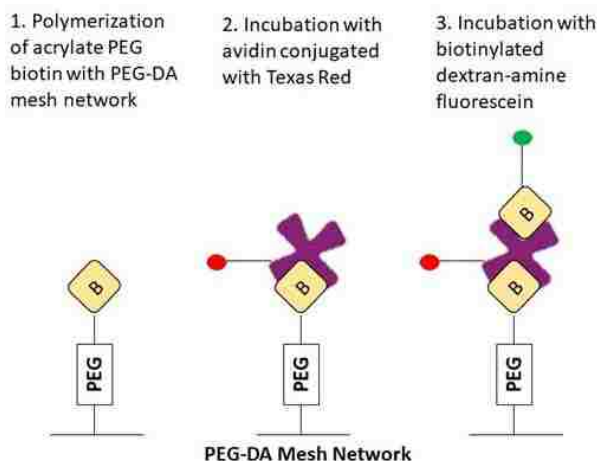
Figure 41: Experimental process flow of mock sandwich immunoassay

To confirm the presence of these biotinylated structures, fluorescent avidin was incubated in the channel. Additionally, to more closely mimic sandwich immunoassays, which utilize antibodies for antigen capture and labelling, biotinylated dextran amine molecules tagged with fluorescein was incubated in the channel after the avidin. The biotinylated molecules here mimic antibodies with avidin mimicking an antigen (Fig. 41).

After printing the channel, the channel was incubated with a 1% BSA for 30 minutes to prevent non-specific binding. Then the channel was incubated with avidin conjugated with Texas Red dye (50 μM) for 30 minutes and subsequently washed with PBS for 30 minutes and imaged with a

fluorescence microscope. The avidin was supposed to bind only to the biotin on the biosensor strips. The fluorescence image and its corresponding fluorescence intensity plot profile indicates that avidin indeed interacted only with the biosensor strips since only the strips were highly fluorescent (Fig. 42A). The channel was then incubated with biotinylated dextran amine tagged with fluorescein (200 µM) for 30 minutes and then washed and imaged. The fluorescence image and its corresponding fluorescence intensity plot profile indicates that the fluorescent biotin interacted only with the avidin within the biosensor strips (Fig. 42B). This indicates that the biosensor strips were able to facilitate the mock sandwich immunoassay shown in Fig. 41. It is not yet confirmed whether the majority of the binding of the avidin and biotin is occurring on the surface of the biosensor strips or within the bulk. Transport studies with this resin need to be performed to assess this.
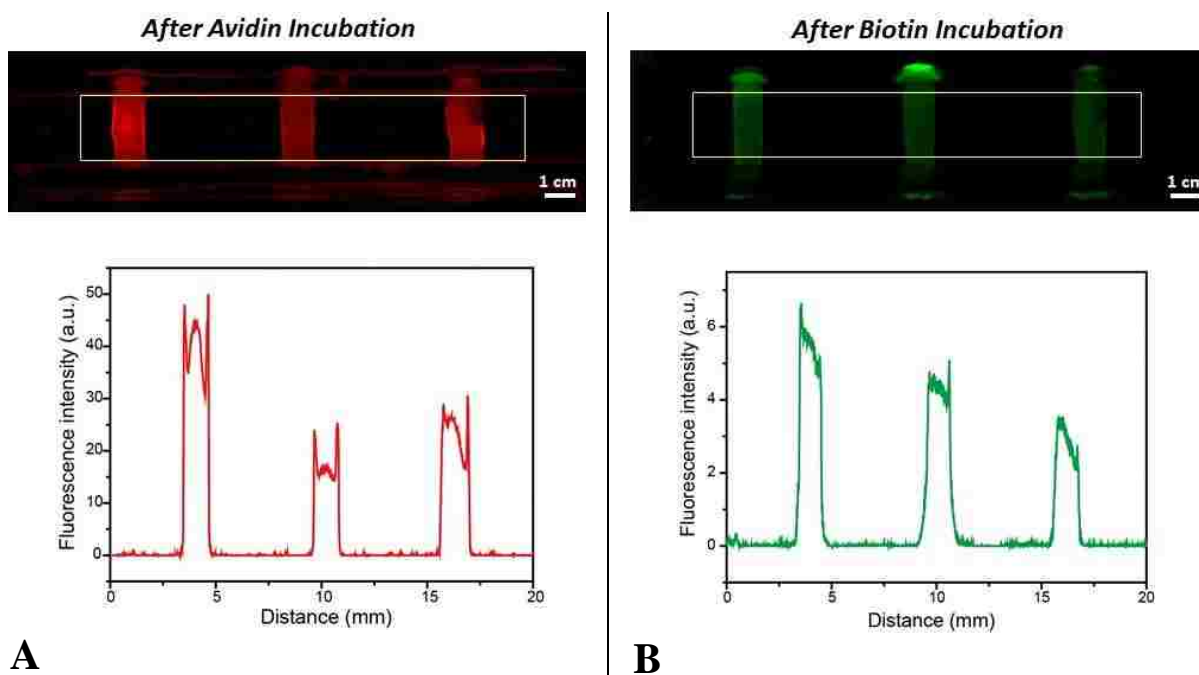
Figure 42: Mock sandwich immunoassay results. (A) Fluorescence image and intensity profile after incubation with avidin conjugated with Texas Red. (B) Fluorescence image and intensity profile after incubation with biotinylated dextran amine tagged with fluorescein.

5.5 Conclusions

Multi-material SL was utilized to fabricate three biosensor strips within a microchannel. This method entailed the switching between two photopolymerizable resins, one resin to build the microchannel and a biosensor resin to fabricate the sensor strips that contained avidin as a model protein. The original biosensor resin composition was not porous, so biotin-binding assays could not be performed. The biosensor resin was modified by adding PEG-8000 as a porogen and covalently bonding biotinylated molecules to the mesh network. This resin was able to be printed in a microchannel and was able to be used for a biotin-binding assay. The experiments shown here illustrate that 3D printing is a facile method to produce microfluidic devices with biosensing capabilities without the need for complex assembly, alignment, or high expertise.

6. Future Research Work

6.1 Introduction

The research work presented herein presents the use of digital manufacturing techniques for the fabrication of microfluidic devices to be used in medical and biological applications. Laser micromachining and 3D printing were shown to be able to produce microfluidic devices with faster fabrication times and less manual labor than conventional photolithography and soft lithography.

A laser micromachining system, VLS 3.60, was characterized to see the dimensions of channels it could produce under different cutting settings. Channels with widths and depths between 50 and 100 μm were reliably produced with this system. Features less than 50 μm in width and depth can be produced with this system but the channels produced were not contiguous because the laser was operating at its extremes.

Laser cutting systems were used to manufacture a personalized microfluidic drug testing platform called OncoSlice whose purpose is to find optimal drug therapies for individual patients. The device holds solutions of drugs in large wells and delivers the drugs to a central chamber containing tissue samples to test their efficacy. Channels were engraved onto a PMMA sheet that was then sealed with another PMMA film that was cut by a laser. A modified 40-well plate of PMMA that holds the drugs was also cut by a laser and bonded to the channel network layer using solvent bonding. An all-plastic device therefore was developed and was easily amenable to design changes. However, the uniformity of channel features in this device can be improved.

SL printing was utilized to fabricate a microchannel that consisted of two different resins. One resin was used to build a microchannel with connectors that could interface with tubing. The other resin was used to print strips of a biosensor within the microchannel. We demonstrated that the strips could entrap or covalently bind proteins, which could be used to detect molecules or cells of interest. The results obtained for SL printing of biosensors in microchannels were very preliminary, but it has the potential to lead to more complex sensor designs that are easier to manufacture and are not realizable with soft lithography.

6.2 Producing Channels with Smaller Dimensions and Higher Precision

The VLS 3.60 system used in the research presented here has a 30 W laser source. A laser source with lower power would yield channels of smaller dimensions if the same power and speed settings are used as with the 30 W system. ULS products are designed to easily change laser sources, so experimenting with a lower power system and characterizing the dimensions of channels would be simple to do.

The engraved channels on the PMMA channel network layer of the OncoSlice have highly complex features such as serpentine, curving channels. The curves for each channel are not entirely uniform leading to slight differences in hydraulic resistance from channel to channel. The binary channels leading to the single outlet also contain many small curves that do not maintain the same curvature. Again, this changes each binary's hydraulic resistance. The channel features are also spaced close together. For example, the open drug lanes are only 500 μm apart from center-to-

center. The small curvatures and the small spacing between features pushed the beam positioning system of the laser close to its limit, so these features were not always uniform. A more accurate laser system that has repeatable movements would alleviate these discrepancies.

The VLS 3.60 system is a basic, entry-level laser system. Universal Laser Systems offers more high-performance laser systems such as the ULTRA 9 and the XLS product line. These systems provide more precise, repeatable beam movements and have friction-free motion systems that prevents vibrations. These features could maintain not only more reproducible, consistent curvatures in the delivery channels and the binary channels, but also more reproducible channel profiles. These systems are also able to house multiple lasers. The ULTRA 9, for example, can hold three lasers: two interchangeable CO_2 lasers and one fiber laser. The CO_2 lasers can be both either 9.3 or 10.6 μm lasers or a combination of both. The fiber laser has a wavelength of 1.06 μm. These wavelengths can also be combined to create a single coaxial beam. Experimenting with these different laser configurations would have to be done to see if smaller channel dimensions can be achieved and if different cross-sectional channel profiles can be achieved.

6.3 Personal Microfluidic Drug Testing Platforms

Laser micromachining was chosen as the method of fabrication for the OncoSlice device because the size of the device is not suitable for most SL printing build platforms. This method is more high-throughput compared to conventional soft lithography. Higher-throughput manufacturing methods are available such as injection molding. Injection molding is not very labor intensive and can process materials quickly, however, it requires the design of a master mold and formation of microchannels is difficult. Consequently, we envision the possibility of using a combination of injection molding and laser micromachining for commercial mass manufacturing of the OncoSlice device. The well plate can be injection molded with a blank bottom that can later have the delivery channels and lanes engraved with a laser. The bottom can then be sealed using solvent bonding.

The fabrication protocol described here for fabricating the OncoSlice device utilizes a hydraulic heat press for many steps. The heat press used was a manual press that has a hand lever that pushes the platens together. The press does not maintain one pressure for a very long time, so the lever must be pulled often to return the press to the desired pressure. The step for sealing the channel network layer with a film was very sensitive to pressure since a slight change probably changed the overall cross-section of the channels in different areas leaving non-uniform cross-sections. At times, too much pressure can cause the film to push into the channels and occlude them. An automated press that maintains the desired pressure during the entire duration of bonding the substrates would be ideal to ensure that each channel network layer substrate was being pressed the same way.

Though the drug testing platform described here illustrates application of single drugs in solution or multiple drugs mixed in solution, it does not allow for sequential application of different drugs at different timepoints. Theoretically, the PTFE membrane with tissue can be picked up and rotated 90 degrees to achieve a grid pattern of cross-combinations of drugs on the tissue. Manual handling of the membrane, however, is difficult. A new design of the OncoSlice that allows for easier

rotation of the membrane would provide a more beneficial platform since more optimal therapies involving sequential application of drugs can be discovered.

Additionally, the porous PTFE membrane is currently manually cut out of a 6-well cell culture insert. This step is difficult and any folds that occur while cutting would not allow the membrane to seal the drug lanes during device use. Since the 40-well plate design can be easily changed by changing the CAD design, the plate can be redesigned to fit an entire cell culture insert and preclude the need for cutting out the membrane.

6.4 Multi-material Stereolithography for Biosensing Applications

Further experimentation with the developed biosensor needs to be done. As mentioned before in section 5.2, the resins developed in this research must be characterized. The pore sizes of the hydrogel can be assessed by observing how molecules of different sizes are able to be transported to the bulk of the resin through diffusion. One way to assess this would be to print two parallel channels that are connected by a porous barrier in between them. The barrier is printed with the resin to be tested. One channel would be filled with a solution with a fluorescent molecule of a specific molecular weight. Taking fluorescence images at different time points can illustrate how long it takes for the molecule to cross the barrier and into the other channel. Testing with different molecular weights would give a range of the molecule size which the barrier can allow through its pores.

A process of printing more than one type of biosensor within a microchannel also has yet to be explored and is difficult to do with our current setup. Selective printing of different hydrogels containing different active biomolecules within a single channel would lead to more complex designs and multiplexed sensing assays.

In the future, it is envisioned that antibodies would be either entrapped or covalently bonded to the PEG-DA mesh and would detect specific cancer biomarkers or cancer cells themselves. Immunoassays can then also be automated and preclude the need for burdensome pipetting using pumps and valves which would facilitate programmed, sequential delivery of reagents. This can perhaps be used in point-of-care diagnostics.

6.5 Conclusion

The OncoSlice device used to be made of many layers of PDMS that had to be carefully aligned and took about four days to fabricate, but currently, laser micromachining has reduced the number of layers to only three and has reduced fabrication time to about two hours. SL allowed for the integration of different functional materials to be fabricated directly within microchannels, which is currently difficult to do with soft lithography.

Digital manufacturing techniques provide easier methods of fabricating microfluidic devices compared to conventional photolithography and soft lithography. Laser micromachining and SL have fast turnaround times and do not require high expertise or excellent hand-eye coordination for assembly of devices and design changes can be made easily through changes in CAD file which are then directly translated to the manufacturing tools. This precludes the need for the fabrication

of new lithographic masks and master molds and significantly reduces costs. I believe that digital manufacturing techniques will in the future become the standard method for building microfluidic devices.

References

1. McDonald, J. C., Duffy, D. C., Anderson, J. R., Chiu, D. T., Wu, H., Schueller, O. J., & Whitesides, G. M. (2000). Fabrication of microfluidic systems in poly(dimethylsiloxane). *Electrophoresis*, *21*(1), 27–40. https://doi.org/10.1002/(SICI)1522-2683(20000101)21:1<27::AID-ELPS27>3.0.CO;2-C
2. Lake, M., Lake, M., Narciso, C., Cowdrick, K., Storey, T., Zhang, S., … Hoelzle, D. (2015). Microfluidic device design, fabrication, and testing protocols. *Protocol Exchange*. https://doi.org/10.1038/protex.2015.069
3. Unger, M. A., Unger, M. A., Chou, H., Thorsen, T., Scherer, A., & Quake, S. R. (2013). Monolithic Microfabricated Valves and Pumps by Multilayer Soft Lithography, *113*(2000), 113–116. https://doi.org/10.1126/science.288.5463.113
4. Ma, Y., Thiele, J., Abdelmohsen, L., Xu, J., & Huck, W. T. S. (2014). Biocompatible macro-initiators controlling radical retention in microfluidic on-chip photo-polymerization of water-in-oil emulsions. *Chem. Commun.*, *50*(1), 112–114. https://doi.org/10.1039/C3CC46733C
5. Gross, B. C., Erkal, J. L., Lockwood, S. Y., Chen, C., & Spence, D. M. (2014). Evaluation of 3D printing and its potential impact on biotechnology and the chemical sciences. *Analytical Chemistry*, *86*(7), 3240–3253. https://doi.org/10.1021/ac403397r
6. Chryssolouris, G., Mavrikios, D., Papakostas, N., Mourtzis, D., Michalos, G., & Georgoulias, K. (2009). Digital manufacturing: History, perspectives, and outlook. *Proceedings of the Institution of Mechanical Engineers, Part B: Journal of Engineering Manufacture*, *223*(5), 451–462. https://doi.org/10.1243/09544054JEM1241
7. Guckenberger, D. J., de Groot, T. E., Wan, A. M. D., Beebe, D. J., & Young, E. W. K. (2015). Micromilling: a method for ultra-rapid prototyping of plastic microfluidic devices. *Lab Chip*, *15*(11), 2364–2378. https://doi.org/10.1039/C5LC00234F
8. Li, H., Fan, Y., Kodzius, R., & Foulds, I. G. (2012). Fabrication of polystyrene microfluidic devices using a pulsed CO2 laser system. *Microsystem Technologies*, *18*(3), 373–379. https://doi.org/10.1007/s00542-011-1410-z
9. Au, A. K., Bhattacharjee, N., Horowitz, L. F., Chang, T. C., & Folch, A. (2015). 3D-printed microfluidic automation. *Lab Chip*, *15*(8), 1934–1941. https://doi.org/10.1039/C5LC00126A
10. Lee, Y.-S., Bhattacharjee, N., & Folch, A. (2018). 3D-printed Quake-style microvalves and micropumps. *Lab on a Chip*, *18*, 1207–1214. https://doi.org/10.1039/C8LC00001H
11. Yuen, P. K. (2008). SmartBuild–A truly plug-n-play modular microfluidic system. *Lab on a Chip*, *8*(8), 1374. https://doi.org/10.1039/b805086d
12. Lee, K. G., Park, K. J., Seok, S., Shin, S., Kim, D. H., Park, J. Y., … Lee, T. J. (2014). 3D printed modules for integrated microfluidic devices. *RSC Adv.*, *4*(62), 32876–32880. https://doi.org/10.1039/C4RA05072J
13. Bhargava, K. C., Thompson, B., & Malmstadt, N. (2014). Discrete elements for 3D microfluidics. *Proceedings of the National Academy of Sciences*, *111*(42), 15013–15018. https://doi.org/10.1073/pnas.1414764111
14. https://www.asiga.com/products/printers/
15. https://formlabs.com/3d-printers/form-2/
16. https://fslaser.com/Products/Printers
17. Khan Malek, C. G. (2006). Laser processing for bio-microfluidics applications (part I). *Analytical and Bioanalytical Chemistry*, *385*(8), 1362–1369. https://doi.org/10.1007/s00216-006-0517-z
18. Malek, C. G. K. (2006). Laser processing for bio-microfluidics applications (part II). *Analytical and Bioanalytical Chemistry*, *385*(8), 1362–1369. https://doi.org/10.1007/s00216-006-0517-z
19. Nayak, N. C., Lam, Y. C., Yue, C. Y., & Sinha, A. T. (2008). CO2-laser micromachining of PMMA: The effect of polymer molecular weight. *Journal of Micromechanics and Microengineering*, *18*(9). https://doi.org/10.1088/0960-1317/18/9/095020

20. Ogilvie, I. R. G., Sieben, V. J., Floquet, C. F. A., Zmijan, R., Mowlem, M. C., & Morgan, H. (2010). Reduction of surface roughness for optical quality microfluidic devices in PMMA and COC. *Journal of Micromechanics and Microengineering*, *20*(6). https://doi.org/10.1088/0960-1317/20/6/065016

21. Klank, H., Kutter, J. P., & Geschke, O. (2002). CO2-laser micromachining and back-end processing for rapid production of PMMA-based microfluidic systems. *Lab on a Chip*, *2*(4), 242. https://doi.org/10.1039/b206409j

22. Wang, Z. K., Zheng, H. Y., Lim, R. Y. H., Wang, Z. F., & Lam, Y. C. (2011). Improving surface smoothness of laser-fabricated microchannels for microfluidic application. *Journal of Micromechanics and Microengineering*, *21*(9). https://doi.org/10.1088/0960-1317/21/9/095008

23. Jensen, M. F., Noerholm, M., Chrstensen, L. H., & Geschke, O. (2003). Microstructure fabrication with a CO2 laser system: characterization and fabrication of cavities produced by raster scanning of the laser beam. *Lab on a Chip*, *3*(4), 302. https://doi.org/10.1039/b308153b

24. Keramas, G., Perozziello, G., Geschke, O., & Christensen, C. B. V. (2004). Development of a multiplex microarray microsystem. *Lab on a Chip*, *4*(2), 152–8. https://doi.org/10.1039/b313472e

25. Qi, H., Wang, X. S., Chen, T., Ma, X. M., & Zuo, T. C. (2009). Fabrication and characterization of a polymethyl methacrylate continuous-flow PCR microfluidic chip using CO2 laser ablation. *Microsystem Technologies-Micro-and Nanosystems-Information Storage and Processing Systems*, *15*(7), 1027–1030. https://doi.org/10.1007/s00542-009-0843-0

26. Skolimowski, M., Nielsen, M. W., Emnéus, J., Molin, S., Taboryski, R., Sternberg, C., … Geschke, O. (2010). Microfluidic dissolved oxygen gradient generator biochip as a useful tool in bacterial biofilm studies. *Lab on a Chip*, *10*(16), 2162. https://doi.org/10.1039/c003558k

27. Chang, T. C., Mikheev, A. M., Huynh, W., Monnat, R. J., Rostomily, R. C., & Folch, A. (2014). Parallel microfluidic chemosensitivity testing on individual slice cultures. *Lab Chip*, *14*(23), 4540–4551. https://doi.org/10.1039/C4LC00642A

28. Pasirayi, G., Auger, V., M. Scott, S., K.S.M. Rahman, P., Islam, M., O'Hare, L., & Ali, Z. (2011). Microfluidic Bioreactors for Cell Culturing: A Review. *Micro and Nanosystemse*, *3*(2), 137–160. https://doi.org/10.2174/1876402911103020137

29. Vlachopoulou, M. E., Tserepi, A., Pavli, P., Argitis, P., Sanopoulou, M., & Misiakos, K. (2009). A low temperature surface modification assisted method for bonding plastic substrates. *Journal of Micromechanics and Microengineering*, *19*(1). https://doi.org/10.1088/0960-1317/19/1/015007

30. Tsao, C. W., & DeVoe, D. L. (2009). Bonding of thermoplastic polymer microfluidics. *Microfluidics and Nanofluidics*, *6*(1), 1–16. https://doi.org/10.1007/s10404-008-0361-x

31. Thompson, B. L., Ouyang, Y., Duarte, G. R. M., Carrilho, E., Krauss, S. T., & Landers, J. P. (2015). Inexpensive, rapid prototyping of microfluidic devices using overhead transparencies and a laser print, cut and laminate fabrication method. *Nature Protocols*, *10*(6), 875–886. https://doi.org/10.1038/nprot.2015.051

32. Vandenburg, H. J., Clifford, A. A., Bartle, K. D., Carlson, R. E., Carroll, J., & Newton, I. D. (1999). A simple solvent selection method for accelerated solvent extraction of additives from polymers. *The Analyst*, *124*(11), 1707–1710. https://doi.org/10.1039/a904631c

33. Koesdjojo, M. T., Koch, C. R., & Remcho, V. T. (2009). Technique for microfabrication of polymeric-based microchips from an SU-8 master with temperature-assisted vaporized organic solvent bonding. *Analytical Chemistry*, *81*(4), 1652–1659. https://doi.org/10.1021/ac802450u

34. Bamshad, A., Nikfarjam, A., & Khaleghi, H. (2016). A new simple and fast thermally-solvent assisted method to bond PMMA-PMMA in micro-fluidics devices. *Journal of Micromechanics and Microengineering*, *26*(6). https://doi.org/10.1088/0960-1317/26/6/065017

35. Melchels, F. P. W., Feijen, J., & Grijpma, D. W. (2010). A review on stereolithography and its applications in biomedical engineering. *Biomaterials*, *31*(24), 6121–6130. https://doi.org/10.1016/j.biomaterials.2010.04.050

36. Mandon, C. A., Blum, L. J., & Marquette, C. A. (2016). Adding Biomolecular Recognition Capability to 3D Printed Objects. *Analytical Chemistry*, *88*(21), 10767–10772. https://doi.org/10.1021/acs.analchem.6b03426
37. Kim, Y. T., Castro, K., Bhattacharjee, N., & Folch, A. (2018). Digital manufacturing of selective porous barriers in microchannels using multi-material stereolithography. *Micromachines*, *9*(3). https://doi.org/10.3390/mi9030125
38. Lee, A. G., Arena, C. P., Beebe, D. J., & Palecek, S. P. (2010). Development of macroporous poly(ethylene glycol) hydrogel arrays within microfluidic channels. *Biomacromolecules*, *11*(12), 3316–3324. https://doi.org/10.1021/bm100792y